UNIVERSIDAD AUTÓNOMA DE NUEVO LEÓN

FACULTAD DE CIENCIAS QUÍMICAS

Adsorption of methylene blue, Congo red, and methyl orange in aqueous solutions by MOF Co-Cl and Co-Br

Presentado por:

Martín Martínez Salazar

Como requisito parcial para obtener el grado de:

MAESTRIA EN CIENCIAS CON ORIENTACIÓN EN QUÍMICA Y TECNOLOGÍA AMBIENTAL

AGOSTO 2025

Acknowledgments

I am mainly grateful to the Facultad of Ciencias Químicas for the support provided during the whole project and for the lessons they taught me for my professional development. I also want to thank CONAHCYT for giving me the scholarship (CVU No. **1315259**). Thanks to my thesis director, Dr. Luis Arturo Obregón Zúñiga, and co-director, Dr. Norma Tiempos Flores, for their invaluable guidance, support, and dedication throughout this project. Their words of encouragement and belief in my work motivated me to overcome challenges along the way.

I would also like to extend my sincere gratitude to Dr. Eugenio Hernández Fernández and Dr. Gloria Lourdes Dimas Rivera for their support. Beyond their technical contributions, I truly appreciate their generosity, patience, and the motivation they provided during this process. I deeply appreciate the time they dedicated to supporting me both academically and emotionally.

Finally, I would like to express my gratitude to my friends in the Organic Synthesis Group for their invaluable advice and shared knowledge. Luis, Iván, Karolina, Tadeo, Mónica, Katia, Goyo, Efren, David, Diana, Camila, Derian, and Fátima, whose friendship went beyond the academic aspects, their friendship brought laughter, motivation, and unforgettable experiences that made this process much more enjoyable.

A special thank you to Leslie and Denisse for their dedication, enthusiasm, and invaluable assistance throughout this project. Their hard work and support in the laboratory were essential in many stages of this research. I deeply appreciated not only their contributions to this research but also the warmth and friendship they brought into this journey. Their presence made the road easier, and for that, I will always be grateful.

Dedication

To my beloved parents, María Elena Salazar Moreno and Martín Martínez Salazar, whose support, love, and encouragement have been the foundation of this journey. From the very beginning, you believed in me and in my decision to pursue a master´s degree, even when the path was uncertain and challenging. Your endless patience, sacrifices, and words of motivation gave me the strength to move forward, even in the most difficult moments.

This work is dedicated to you, with all my love and gratitude.

Resumen

Monterrey, Nuevo León

Abril, 2025

Universidad Autónoma de Nuevo León

Facultad de Ciencias Químicas

Título del estudio: **Adsorption of methylene blue, Congo red, and methyl orange in aqueous solutions by MOF Co-Cl and Co-Br**

Área de estudio: Química y Tecnología Ambiental

Número de páginas: 68

Propósito y método de estudio: Dentro de los mayores contaminantes del agua se tienen a los colorantes cuya producción anual a nivel mundial es de más de 2 millones de toneladas, debido a sus usos en la industria plástica, comida, papel, textil, cosmética y farmacéutica. Muchos de los tintes encontrados en aguas residuales provenientes de la industria son tóxicos y carcinogénicos, además de que pueden interferir en los procesos fotosintéticos. Por tal motivo, en el presente proyecto se realizó la síntesis de dos nuevas estructuras metal-orgánicas y su aplicación en la remoción de colorantes (azul metileno, rojo Congo y naranja de metilo) en solución acuosa.

Contribuciones y conclusiones: Se realizó la síntesis de dos nuevas estructuras metal-orgánicas (MOF, por sus siglas en inglés) mediante la coprecipitación de ligantes de imidazol con cobalto como metal central, a temperatura ambiente. Los estudios de pH, cinéticos e isotérmicos permitieron analizar en detalle las interacciones entre los colorantes y las MOF. Para **Co-Cl**, se obtuvieron capacidades de adsorción máximas de 119 mg/g, 265 mg/g y 1800 mg/g para azul de metileno, naranja de metilo y rojo Congo, respectivamente. En el caso de **Co-Br**, las capacidades fueron de 61 mg/g, 247 mg/g, y 2100 mg/g para los mismos colorantes. Estos resultados destacan el potencial de las estructuras sintetizadas para su aplicación en procesos de tratamiento de agua.

_____

Dr. Luis Arturo Obregón Zúñiga

Director de tesis

Summary

Monterrey, Nuevo León

April, 2025

Universidad Autónoma de Nuevo León

Facultad de Ciencias Químicas

Title´s study: **Adsorption of methylene blue, Congo red, and methyl orange in aqueous solutions by MOF Co-Cl and Co-Br**

Field of study: Environmental chemistry and technology

Number of pages: 68

Purpose and Study Methods: The substances coming from discharges of the industrial field are the dyes. The annual production worldwide is more than 2 million tons, due to their use in the plastic, food, paper, textiles, cosmetics, and pharmaceutical industries. Many of the dyes found in industrial wastewater are toxic and carcinogenic. Therefore, during the present project, the synthesis of new metal-organic frameworks and its application in dye removal (methylene blue, Congo red, and methyl orange) in aqueous solution was carried out.

Contributions and Conclusions: The synthesis of two new metal-organic frameworks (MOFs) was carried out via coprecipitation of imidazole ligands with cobalt as the central metal at room temperature. Additionally, adsorption tests were conducted in batch systems to evaluate the retention capacity of the dyes methylene blue, methyl orange, and Congo red. pH, kinetic, and isotherm studies provided insights into the interactions between the dyes and the MOFs. For **Co-Cl**, maximum adsorption capacities of 119 mg/g, 265 mg/g, and 1800 mg/g were obtained for methylene blue, methyl orange, and Congo red, respectively. In the case of **Co-Br**, the capacities were 61 mg/g, 247 mg/g, and 2100 mg/g for the same dyes. These results highlight the potential of the synthesized structures for application in industrial water treatment processes.

_____

Dr. Luis Arturo Obregón Zúñiga

Advisor

Adsorption of methylene blue, Congo red, and methyl orange in aqueous solution by MOF Co-Cl and Co-Br

Presented by:

Martín Martínez Salazar

The present research project was done at Laboratorio de Química Industrial, of Centro de Laboratorios Especializados (CELAES) of Facultad de Ciencias Químicas, UANL, under the supervision of Dr. Luis Arturo Obregón Zúñiga and Dr. Norma Tiempos Flores, with resources given by Consejo Nacional de Humanidades, Ciencias y Tecnologías (CONAHCYT) with the scholarship 1315259.

Table of contents

List of Figures

List of tables

CHAPTER 1 INTRODUCTION

1.1. Introduction

Water pollution and shortage are environmental problems that are important for human society where the main challenge is its conservation and proper use (1). The discharge of toxic and hazardous substances is the main threat to aquatic ecosystems. Mainly, discharges come from industrial processes, daily human activities, and agriculture. Dyes are among the substances discharged by industrial processes. The annual production worldwide is more than 2 million tons, due to their use in the plastic, food, paper, textiles, cosmetics, and pharmaceutical industries. Worldwide, the textile industry uses more than 10,000 tons of dyes per year, generating many different wastes containing high concentrations of dyes that are discharged into streams (2). Many of the dyes found in industrial wastewater are toxic and carcinogenic. Some of the most common dyes are methylene blue (MB) (3), Congo red (CR) (4), and methyl orange (MO) (5). Commonly, these dyes can cause several health problems such as skin irritation, eye irritation, respiration problems disease, sneezing, and cancer (6). According to Mexican regulation NOM-165-ECOL-1994, the maximum permissible limit for dyes and pigments coming from the discharge of industries is 200 mg/L. In this sense, it is necessary to reduce the concentration of the dyes and remove them from wastewater.

There are several methods for dye removal, some of them are electrocoagulation, advanced oxidation techniques (AOT), membrane separation, and adsorption (7). However, the implementation of the AOT and membrane separation are highly costly in terms of energy consumption and generation of byproducts (8). The adsorption is the most effective for the removal of inorganic substances and organic contaminants from effluents due to its ease of operation, low cost, high efficiency, and lack of byproducts (9). However, scientists look for adsorbents that present hydrophobic properties, high specific surface areas, porosity, and thermal and chemical stability.

One of the best adsorbents used is activated carbon (AC) because of its high adsorption efficiency, high surface area, and large pores in its structure; however, it is a very expensive adsorbent due to its high production and regeneration costs (10).

In addition, it presents difficulties in the separation of water and generates secondary contamination. Therefore, the search continues for alternatives materials with desirable properties such as high surface area and large pores, like zeolites and clays (11).

Metal-organic frameworks (MOFs) are a class of porous materials formed by three and two-dimensional networks of metal complexes with organic ligands. Because of their high specific surface area and uniform and modifiable pore size, they are considered potential materials for adsorption, separation, and catalysis (12). In this regard, zeolitic imidazole frameworks (ZIFs) are a class of MOFs, formed by transition metal cations, commonly Zn (II) and Co (II), and imidazole derivatives as ligands, which possess high thermal and chemical stability (13). Particularly, Co-MOFs exhibit better pH stability and higher surface areas than Zn-MOFs depending on the synthesis conditions. These properties make them better candidates for adsorption processes.

Another key factor in adsorption is the hydrophobicity of the adsorbent. Hydrophobic adsorbents do not interact with water molecules, enhancing the interaction between the adsorbent and adsorbate. The water contact angle (θ_w) is a parameter that measures the angle formed between the solid and liquid surface (14). High values of θ_w (>90°) refer to hydrophobic adsorbents and lower values (<90°) are considered hydrophilic (15).

ZIF-71 and **ZIF-71(ClBr)** are MOFs, formed by Zn (II) as central metal atom and ligands of 4,5-dichloroimidazole and 4-bromo-5-chloroimidazole, that present high surface areas of 1000 m^2/g and 969 m^2/g as well as being classified as hydrophobic materials with θ_w of 108° (16) and 126.79° (17), respectively. Thus, the present project proposes the synthesis of analogs of these ZIFs with the modification of the metal atom of Zn by Co (**Co-Cl** and **Co-Br**) (**Figure 1**) expecting an increment in the surface area of the MOFs and as a result enhancing the adsorption of different types of dyes such as methylene blue, Congo red and methyl orange with high adsorption capacities (q_m).

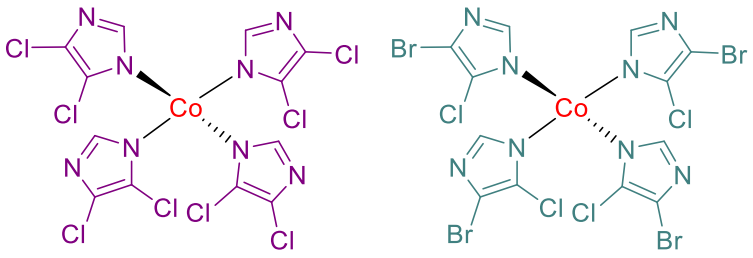

Figure 1. Structures of **Co-Cl** and **Co-Br**.

1.1. Background

During the past few years, the removal of dyes has been widely investigated **Table 1**. The use of activated carbons from waste as adsorbents are excellent candidates because they exhibit high adsorption capacities. These types of adsorbents require high-temperature conditions (>500°C) for their synthesis to obtain materials with high surface areas above 1000 m^2/g.

Among all ZIFs, **ZIF-8** and **ZIF-67** (**Figure 2**) are the most studied and used for the adsorption of pollutants owing to the high surface areas such as 1200 m^2/g (18) and 1700 m^2/g (19), respectively, depending on the different conditions of synthesis with low-temperature conditions (<50°C) (20). **ZIF-8** presents a high-water contact angle (θ_w) of 97° and **ZIF-67** is 58°(21). Due to its hydrophobic nature, **ZIF-71** has also been evaluated for Congo red removal (22), as well as **ZIF-71 (ClBr)** for the adsorption of butanol.

Table 1. Reported adsorbents on the adsorption of MB, CR and MO

Dye	Adsorbent	Surface area (m^2/g)	Adsorbent amount (g)	Time (min)	Adsorption capacity (mg/g)	Reference
MB	AC from sugarcane	N.R.	0.05	90	51.00	(23)
	AC from Lignocellulosic agriculture wastes	2490	0.05	60	158.90	(24)
	ZIF-8	538	0.05	120	24.57	(20)
	ZIF-67	594	0.05	100	57.14	(25)
	ZIF-8/PAN	N.A.	0.005	360	120.48	(26)
	Commercial AC	950	0.1	50	200.00	(27)
MO	AC from orange and lemon peels wastes	168	0.8	180	33.00	(10)
	ZIF-8	1200	0.01	180	322.58	(28)
	ZIF-67	594	0.05	90	75.58	(25)
	AC from sugarcane	1073	0.01	50	161.80	(29)
	Commercial AC	653	0.01	85	77.10	
	ZIF-67	1676	0.02	120	1342.00	(30)
CR	AC from cardamom peels	N.R.	1.0	60	69.93	(31)
	AC from Jujube seed	N.R.	1.0	120	75.76	(32)
	ZIF-67	1388	0.2	140	714.30	(33)
	ZIF-8	1200	0.01	100	1250.00	(34)
	Commercial AC	494	1.0	90	300.00	(35)

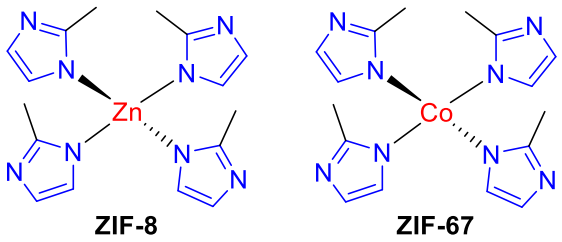

ZIF-8 **ZIF-67**

Figure 2. Structures of **ZIF-8** and **ZIF-67**

As summarized in **Table 1**, the surface area plays an important role that affects the adsorption capacity of the adsorbent on the dyes. As the surface area of the

adsorbent increases, so does the adsorption capacity toward dyes. This is attributed to a large number of sorption sites between the adsorbent and dye. The amount of adsorbents used and contact time are important parameters for the evaluation of the adsorbents. There are no specific required values for these parameters; however, adsorbents that exhibit high adsorption capacities using the least amount of adsorbent with the shortest contact time are highly demanded.

1.2. **Critical analysis**

In the literature, activated carbons present high adsorption capacities utilizing amount of adsorbent from 0.01-0.4 g with short times of 50-180 min against the three types of dyes due to their high surface area from 600-2500 m^2/g, and this property enhances the adsorption of dyes as it increases. The precursors of activated carbons come mainly from wastes that are reused for beneficial applications such as dye adsorption. However, these carbons require high-temperature synthesis conditions like more than 500°C, and produce high energy costs.

Therefore, alternative options such as MOFs have been used during the past years, **ZIF-8** and **ZIF-67** present high surface areas from 550-1700 m^2/g, requiring low-temperature conditions (50°C), achieving high adsorption capacities utilizing less amount of adsorbent (0.01-0.05 g) in short times (90-180 min) for the removal of methylene blue, Congo red and methyl orange dye. The metal center in the MOF increases the surface area as it happens between **ZIF-8** and **ZIF-67** even though they present the same ligands but differ in the metal center of Zn (II) and Co (II). However, **ZIF-8** has a high θ_w of 97°, whereas **ZIF-67** is 57°. Despite this, hydrophobicity improves with the modification of the ligands achieving hydrophobic adsorbents such as **ZIF-71** and **ZIF-71 (ClBr)** with high θ_w.

Due to the above, the present project proposes to synthesize **ZIF-71** and **ZIF-71 (ClBr)** with a modification of the metal atom of Zn by Co (**Co-Cl** and **Co-Br**). There is no report of the synthesis of these analogs of the ZIFs with the atom of Co. Then, evaluate the adsorption capacity (q_e) of different types of dyes such as methylene blue, Congo red, and methyl orange.

1.3. **Scientific contribution**

Application of two new adsorbents, **Co-Cl** and **Co-Br,** in the removal of different types of dyes.

1.4. **Hypothesis**

Co-Cl and **Co-Br** exhibit better adsorption capacities in the selected dyes than the reported **ZIF-8** and **ZIF-67**.

1.5. **Objectives**

1.5.1. General Objective

Remove the selected dyes using the metal-organic frameworks derived from imidazole **Co-Cl** and **Co-Br.**

1.5.2. Specific Objectives

- Synthesize ligands **4** and **5** from imidazole.
- Characterize ligands **4** and **5** by FTIR, and high-resolution mass spectrometry (HRMS).

4 **5**

Figure 3. Imidazole derivatives.

- Synthesize the metal-organic frameworks **Co-Cl** and **Co-Br** using the ligands **4** and **5**.
- Characterize the metal-organic frameworks **Co-Cl** and **Co-Br** by powder X-ray diffraction (PXRD), nitrogen physisorption, water contact angle, and FTIR.
- Determine the adsorption capacity in MB, CR, and MO of **Co-Cl** and **Co-Br** by visible spectrophotometry technique.
- Achieve the desorption of MB, CR, and MO from ZIFs.
- Determine the adsorption-desorption cycles of the ZIFs in the dyes.

CHAPTER 2 THEORETICAL FRAMEWORK

2.1. **Water pollution**

Water is an essential component of living things, and its conservation is a problem of significant importance globally, where one main challenge for society is the selective removal of contaminants. According to the World Health Organization (WHO), only 5% of the water worldwide is suitable for consumption (36). In addition, in 2022, 6 billion people used safe drinking water services free from contamination, whereas 2 billion people were without safe water services (36,37). In this sense, several parameters are established in wastewater treatment plants to guarantee water quality that is ideal for consumption.

The General Law of Ecological Balance and Environmental Protection in Mexico (38) defines a contaminant as any matter or energy in any of its physical states and forms, which modifies its composition and natural condition by acting with water. The most common pollutants in wastewater include heavy metals (39), dyes (40), pesticides (41), herbicides (42), and pharmaceuticals (43).

2.2. **Dyes**

Dyes are chemical substances that provide color to substrates upon application. They are used in color paints, textiles, leather, photographs, cosmetic and pharmaceutical products (44). Dyes are different from pigments, because pigments are generally insoluble in water and most solvents, whereas dyes are soluble in water and solvents. Mainly, dyes are organic compounds instead of pigments that can be either organic or inorganic. The particle size of dyes is smaller than that of pigments. However, pigments last longer than dyes. Therefore, the main difference between dye and pigments is their size and lifetime (45).

2.2.1. Classification of dyes

Dyes can be classified according to their usage adopted by the color index (44) listed in **Table 2**.

Table 2. Classification of dyes.

Type	Solubility in water	Application
Acidic	Mainly soluble	Silk, wool, nylon
Basic	Soluble	Paper
Disperse	Insoluble	Polyester, cellulose, acrylic fibers
Direct	Soluble	Leather, cotton, rayon
Reactive	Soluble	Cotton, cellulosic fibers
Solvent	Insoluble	Plastics, gasoline, lubricants
Sulfur	Soluble	Wood, paper, silk
Vat	Soluble	Cotton, rayon, wool

Some of the common dye pollutants are Congo red (CR), crystal violet (CV), indigo blue (IB), indigo carmine (IC), malachite green (MG), methylene blue (MB), methyl orange (MO), etc. The high solubility in water of these dyes makes them relevant contaminants for wastewater treatment plants. **Figure 4** represents the chemical structures of the common dyes mentioned.

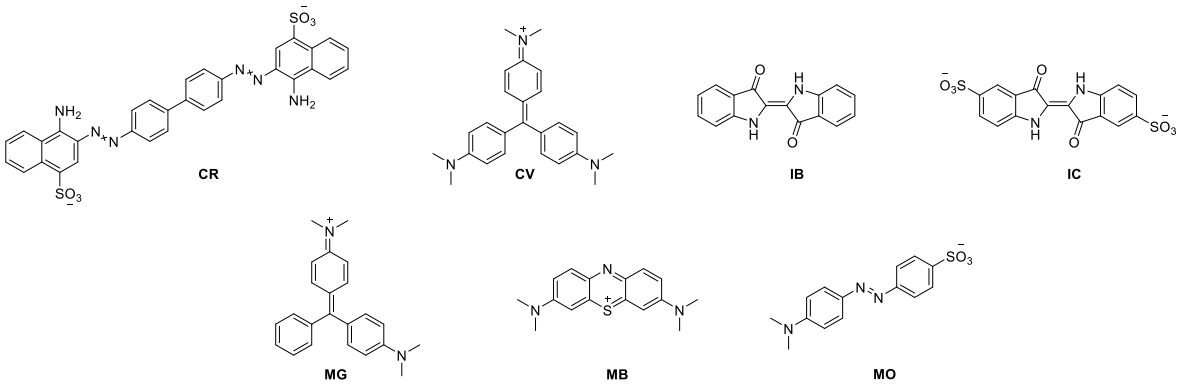

Figure 4. Chemical structures of dyes.

2.3. **Techniques for dye removal**

Scientific researchers have been looking for techniques for dye removal. There are several methods used for treating wastewater to remove dyes. **Table 3** summarizes methods employed for dye removal with their advantages and disadvantages. Among them, the adsorption method is one of the most effective methods for water treatment because of its low operational cost and high efficiency. The adsorbent

doesn´t need pretreatment before its usage. The technique doesn´t generate byproducts that can be harmful to the environment (8,11).

Table 3. Techniques for water remediation

Technique	Advantage	Disadvantage
Membrane separation	Removal of all types of dyes	Sludge production
Photocatalyst	No sludge production	Byproducts formation
Ozonation	Effective decolorization	High operational cost
Fenton reagents	Effective decolorization	Sludge production
Adsorption	Low operational cost	Agglomeration

2.4. **Adsorption**

Adsorption can be classified into two different types based on the interaction between the adsorbate and adsorbent: physical adsorption and chemical adsorption (**Figure 5**) (46). Physical adsorption is also known as physisorption, because of its weak Van der Waals forces between adsorbate and adsorbent. This type of adsorption is a multi-layered and reversible process. Meanwhile, chemical adsorption, known as chemisorption, has a strong chemical bonding between adsorbate and adsorbent. This type of adsorption typically involves monolayer coverage and irreversible interactions.

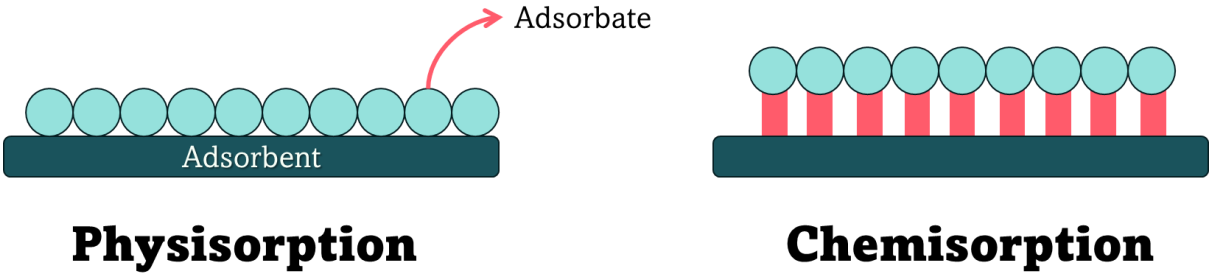

Figure 5. Types of adsorption.

2.5. **Adsorbents**

An adsorbent is a solid substance used to remove contaminants from liquid or gas that can harm the environment. Among the adsorbent materials proposed for dye removal, activated carbon (AC) is the most used for wastewater treatment. AC presents a high surface area and a large volume of pores, therefore its usage in this

type of treatment. However, its high cost of production leads researchers to look for more economical alternatives (47).

From this perspective, other alternatives like zeolites, clays, activated carbons from waste resources, and metal-organic frameworks (MOFs) start to become novel materials for the adsorption process (48).

2.5.1. ZIF

Metal-organic frameworks (MOFs) are a class of porous materials formed by three- and two-dimensional networks of metal complexes with organic ligands (49). The properties of both organic and inorganic components of their structures make MOFs interesting materials for scientific research (50). They present high surface areas from 1000 to 10,000 m^2/g, these values can go over other adsorbents such as activated carbon and zeolites (51,52). All these properties make MOFs to be widely used for gas separation and purification (such as H_2, and CO_2), catalysts, and adsorption (53,54).

Zeolitic imidazole frameworks (ZIFs) are a class of MOFs, formed by transition metal cations, commonly Zn and Co, and imidazole derivatives as ligands, which possess high thermal and chemical stability (20). They consist of a bridge composed of M-Im-M where M is for Zn or Co cation and Im is for the imidazolate linker. The structure is like the conventional zeolites (**Figure 6**), where Zn^{2+} ions are related to silicon and imidazolate anion forms bridges, such as the oxygen in zeolites forming an angle of 145°.

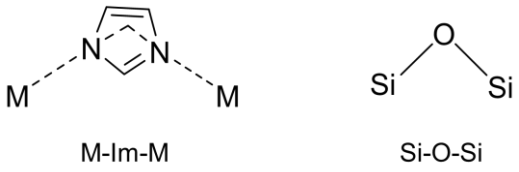

Figure 6. ZIF and zeolites bridging angles of 145°.

ZIFs possess properties of both MOFs and zeolites such as high surface area, high crystallinity, high functionalities, and thermal and chemical stability. These properties make them suitable for a variety of applications, including catalysis, separation, adsorption, and sensing (55,56).

2.6. **Structural characterization**

2.6.1. Fourier Transformed Infrared Spectroscopy (FTIR)

FT-IR spectroscopy consists of measuring the absorption that is radiated from the infrared light. This is related to a change in the dipole moment of the molecule bonds. The intensity of an absorption bond depends on the magnitude of the change in the dipole moment, the greater the change the greater the absorption (57). This change can occur in two types of vibrational modes: stretching and bending (**Figure 7**). Stretching can be symmetric and asymmetric. Bending can be wagging, twisting, rocking, and scissoring. Within a range of wavenumber of 4000-400 cm^{-1} or wavelengths of 2.5-15 mm (57,58).

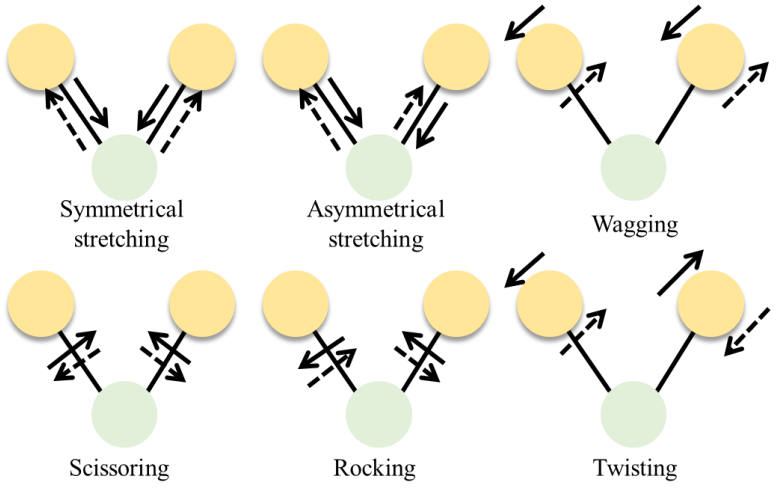

Figure 7. Vibrational modes.

2.6.2. High-Resolution Mass Spectrometry (HRMS)

HRMS consists of using a small amount of sample introduced into the equipment where it is vaporized and ionized forming ions. The mass analyzer sorts the ions by applying electromagnetic fields according to their masses. The resolution of the analyzer plays a key role in this step, as it defines the instrument´s ability to distinguish between ions with very similar mass-to-charge ratios (*m/z*). A high-resolution analyzer can accurately separate and identify compounds with nearly identical molecular weights. Finally, the detector measures the value and provides

data from the abundance of each ion present. This technique enables to determine the exact molecular mass of a sample (57).

2.6.3. Powder X-ray diffraction (PXRD)

PXRD consists of the incidence of an X-ray beam on the flat sample at a certain angle, then the diffracted radiation is collected by a detector placed at all directions of the diffracted rays thus a diffractogram provides information about the diffracted crystalline planes as a function of an angle. This technique works on the principle of Bragg´s equation (**(Eq. *1***), it allows us to study the directions in which X-ray diffraction on the surface of a crystal produces constructive interferences since it allows to predict the angles at which X-rays are diffracted by a crystalline material (59).

$$n\lambda = 2dsin\theta \quad \textbf{(Eq. 1)}$$

Where λ is the X-ray wavelength, d is the spacing of the diffracting planes, and θ is the angle between the incident rays and the diffracting planes.

2.6.4. Nitrogen physisorption

Nitrogen physisorption occurs when a gas interacts with a degassed solid by Van der Waals forces, which can be London type or dipole-dipole, therefore nitrogen is the most used gas. This technique determines the BET surface area using (**(Eq. *2***) and pore distribution of a sample (60,61).

$$S_{BET} = n_m N_A \sigma_m \quad \textbf{(Eq. 2)}$$

Where S_{BET} is the specific surface area, n_m refers to mono-layer capacity, N_A is the Avogadro constant, and σ_m is the cross section of an adsorbed molecule.

2.6.5. Water contact angle

The water contact angle (θ_w) is a measure of the wettability of a surface, defined by the angle formed between the droplet of water and the surface it rests on. It is used to assess the hydrophilic (water affinity) or hydrophobic (water repellency) nature of a material. The materials can be classified (**Figure 8**) as hydrophilic (θ<90°), hydrophobic (θ>90°) and superhydrophobic (θ>150°) (14).

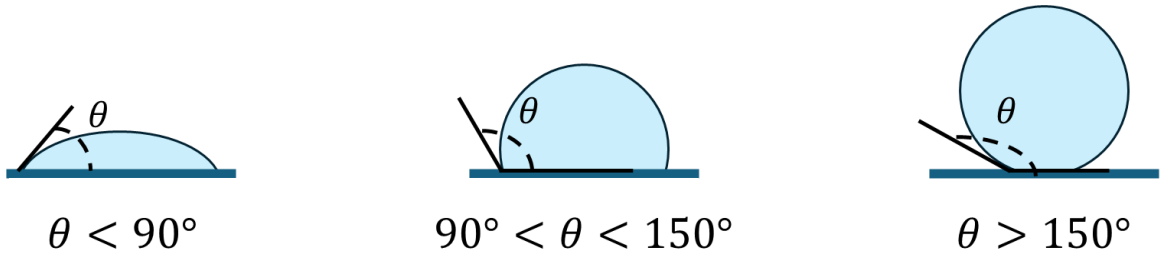

Figure 8. Representative illustration of the droplet on the surface of a material.

It is based on the Young´s equation (**(Eq. *3***), which relates the balance of forces at the three-phase contact line where a liquid, solid, and air meet.

$$\gamma_{sv} = \gamma_{sL} + \gamma_{Lv} cos\theta \qquad \textbf{(Eq. 3)}$$

Where γ_{sv} is the surface energy the solid in contact with the vapor, γ_{sL} is the surface energy of the solid in contact with the liquid, γ_{Lv} surface tension of the liquid and θ is the contact angle.

2.6.6. Point of zero charge (PZC)

The point of zero charge is defined as the pH at which the surface of a material has a net zero charge, meaning the number of positive and negative charges on the surface are equal (62).

The surface of a material defined as **M** can develop a charge because of the protonation or deprotonation reactions in an aqueous environment depending on the pH of the solution.

$$MOH + H^+ \leftrightarrow MOH_2^+$$

$$MOH \leftrightarrow MO^- + H^+$$

The PZC can be determined experimentally by several methods such as acid-base titrations (62), electrochemical (63) and salt addition (64).

2.7. **Visible light spectroscopy (Vis spectroscopy)**

This technique is widely used for analytical media. For a substance to be active in the visible it must be colored, the reason for a substance to have color is that it absorbs certain frequencies or wavelengths of the visible spectrum and transmits

others. This technique works with Lambert-Beer Law (**(Eq. *4*) which states the relationship between absorbance from a dissolved substance is directly proportional to its concentration in a solution (57).

$$Abs = \varepsilon bC \qquad \textbf{(Eq. 4)}$$

Where **Abs** is the absorbance of the substance, $\boldsymbol{\varepsilon}$ is the molar absorption coefficient, **b** is the path length and **C** is the concentration.

CHAPTER 3 METHODOLOGY

3.1. **Materials and methods**

The synthesis of ligands **4a-b**, ZIFs, and adsorption experiments were carried out at the Laboratorio de Química Industrial located at Centro de Laboratorios Especializados of Facultad de Ciencias Químicas (FCQ), Universidad Autónoma de Nuevo León (UANL). The equipment used was a Barnstead/Thermolyne magnetic hot plate, BRANSON 5510 ultrasound bath, Hanna pH meter, and a Labtech LWB-1060 bathtub. Melting points were registered using an Electrothermal Mel-Temp apparatus. Thin Layer Chromatography was performed to follow the progress of the reaction, silica gel plates 60 F_{254} were used and revealed using ultraviolet lamp Spectroline model CM-10.

Ligand structural elucidation was carried out using a Perkin Elmer Spectrum One FT-IR spectrophotometer located at Laboratorio de Análisis Instrumental of FCQ, UANL, and a mass spectrometer Agilent Technologies 1260 Infinity located at Brigham Young University, Utah, USA.

Structural elucidation of ZIFs was carried out using a PANalytical X´Pert Pro for the powder X-ray diffraction (PXRD) located at Laboratorio de Servicios Profesionales of FCQ, UANL. Nitrogen physisorption technique using a Micromeritics Tristar II Plus located at Laboratorio de la Sustentabilidad de los Procesos del Petróleo at División de Estudios de Posgrado from FCQ, UANL. FT-IR analysis was carried out using a Perkin Elmer Spectrum One FT-IR.

3.2. **Reagents and Suppliers**

Table 4. Reagents and Suppliers.

Reagents	Suppliers
Sodium hypochlorite	-
Distilled water, ethyl acetate, hexane, activated carbon, methanol 99.9%	Desarrollo de Especialidades Químicas, S.A. de C.V.
Glacial acetic acid 99.7%, sodium sulfite 98%, conc. Hydrochloric acid	MEYER
Sodium acetate 99.8%, cobalt nitrate pentahydrate, Congo red	CTR SCIENTIFIC
Imidazole 99%, sodium sulfate 99%, sodium hydroxide 98%, celite, bromine, methylene blue, methyl orange	MERCK

3.3. **Synthesis of compounds 2, 3, 4 and 5**

Ligands **4** and **5** were synthesized using imidazole as starting material following the synthetic route shown in **Scheme 1.**

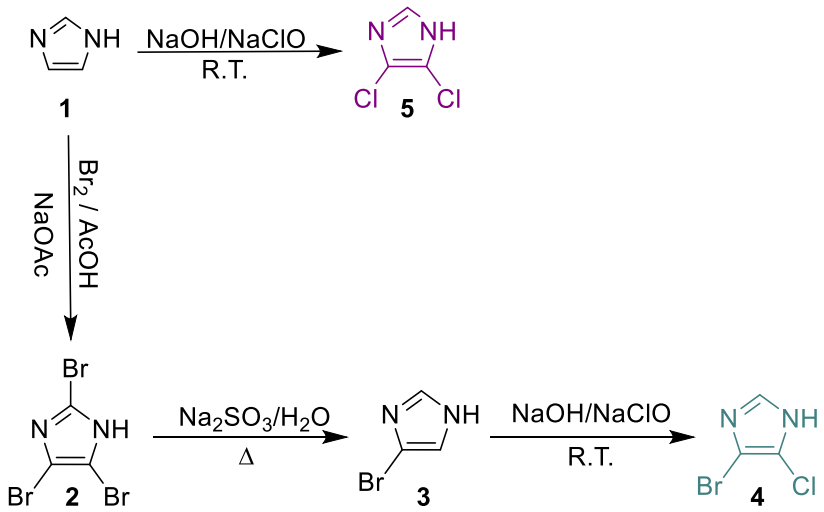

Scheme 1. Synthetic route for ligands **4** and **5**.

*3.3.1. Synthesis of 2,4,5-tribromoimidazole **2***

Imidazole **1** (6.12 g, 89.9 mmol), sodium acetate (66.3 g, 808.1 mmol), and acetic acid (300 mL, 5.2 mol) were added into a 1 L round flask and dissolved with acetic acid (300 mL, 5.2 mol). The reaction mixture was kept stirred for 10 min. Then, a bromine solution (43.1 g, 13.8 mL) in acetic acid (50 mL, 874.2 mmol) was added dropwise over 2 h. The reaction mixture was stirred vigorously overnight at room temperature. Afterward, 500 mL of deionized water was added to the mixture and stirred for 1 h. The precipitate obtained was filtered and washed with 500 mL of water and dried under a vacuum.

*3.3.2. Synthesis of 4-bromoimidazole **3***

In a 500 mL round flask, compound **2** (10 g, 32.8 mmol), sodium sulfite (22.7 g, 180 mmol), and water (250 mL) were added. The mixture was stirred vigorously for 4 h. After the reaction was completed, extractions with ethyl acetate (3 x 30 mL) were performed. The combined organic extracts were dried over anhydrous sodium sulfate and concentrated under reduced pressure.

*3.3.3. Synthesis of 4-bromo-5-chloroimidazole **4***

To a 100 mL Erlenmeyer flask, compound **3** (3.45 g, 19 mmol) and NaOH solution (1.36 g, 34 mmol) dissolved in 16.4 mL of distilled water were added. To the reaction mixture, NaOCl (Clorox 8.25% 32 mL, 477.1 mmol) was added, and the reaction was left in stirring for 80 minutes at room temperature. Afterward, activated carbon (1.0 g, 83.2 mmol) was added to the solution and left to stir for 1 h, after time passed it was filtered and washed with distilled water (100 mL). The obtained solution was adjusted to pH 6-7 with concentrated HCl, the precipitate was filtered and washed with water (100 mL) and dried under vacuum.

*3.3.4. Synthesis of 4,5-dichloroimidazole **5***

In a 100 mL Erlenmeyer flask, compound **1** (5 g, 73.4 mmol) and NaOH solution (2.9 g, 72.5 mmol) dissolved in 35 mL of distilled water were added. To the reaction mixture, NaOCl (Clorox 8.25% 110 mL, 1.6 mmol) was added, and the reaction mixture was left for 60 minutes at room temperature with constant stirring. Activated carbon (1.0 g, 83.2 mmol) was added to the solution and left for 60 min. Then, the

mixture was filtered and washed with distilled water (100 mL). The obtained solution was adjusted to pH 6-7 with concentrated HCl, and the precipitate was filtered and washed with water (100 mL) and dried under vacuum.

3.4. **Synthesis of MOFs Co-Cl and Co-Br**

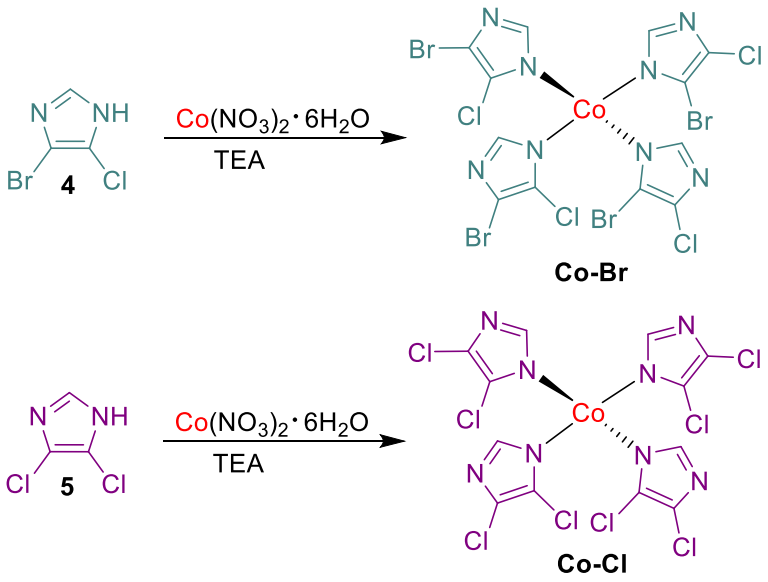

Figure 9. Synthesis of MOFs.

Following the procedure of **Figure 9**, two solutions in 50 mL beakers were prepared. In solution 1, compound **4** or **5** (1 g) and TEA (0.184 g, 2.7 mmol) were dissolved in methanol (20 mL) and sonicated for better dissolution. In solution 2, $Co(NO_3)_2 \cdot 6H_2O$ (0.4 g, 1.4 mmol) were dissolved in methanol (10 mL) and sonicated for better dissolution. Solution 2 was transferred to solution 1 dropwise without stirring. The reaction was left to rest for 24 h. Then, it was centrifuged at 3500 rpm for 6 min and washed with methanol (3 X 5 mL). Finally, the product was dried under a vacuum at 80 °C for 4 h.

3.5. **Adsorption of MB, CR, and MO**

For all dye solutions, standards of 0-15 mg/L were prepared from a stock solution of 100 mg/L of the selected dye. The absorbance vs concentration calibration plot was obtained by Visible spectrophotometry at a maximum wavelength (λ_{max}) of the corresponding dye: for methylene blue (λ_{max} =665 nm) (65), Congo red (λ_{max} =505 nm) (66), and methyl orange (λ_{max} =464 nm) (67). The adsorption capacity (**Eq. 5**)

and the removal percentage (**Eq. 6**) were calculated with the concentrations obtained before and after the adsorption.

$$q = \frac{(C_o - C_f)V}{m} \quad \textbf{(Eq. 5)}$$

$$\% = \frac{C_o - C_f}{C_o} \times 100 \quad \textbf{(Eq. 6)}$$

Where $\mathbf{C_o}$ is the initial adsorbate concentration (mg/L), **q** is the adsorption capacity of the adsorbent (mg/g), $\mathbf{C_f}$ is the final concentration (mg/L), **V** is the adsorbate solution volume (L), and **m** is the mass of the adsorbent (g).

3.5.1. Determination of point of zero charge (PZC)

The point of zero charge was determined by the salt addition method (64) utilizing 0.1 M NaCl solutions. For this experiment, three replicates were performed. In a series of 50 mL Falcon tubes, 50 mg of adsorbent was added to 30 mL of the NaCl solution. The initial pH (pH_i) was adjusted from 4 to 10 utilizing 0.1 M NaOH and 0.1 M HCl. The samples were shaken for 24 h using a Shaker at 200 rpm. After this period, the final pH (pH_f) of each sample was measured. Finally, the PZC was calculated by plotting ΔpH (pH_i-pH_f) against pH_i.

3.5.2. Effect of pH

The experiments were carried out in triplicate. In a 50 mL beaker, 50 mg of adsorbent were added to 30 mL of dye solution with an initial concentration of 30 mg/L. The pH of the solution was varied from 4 to 10 using 0.1 M NaOH and 0.1 M HCl. The samples were kept under constant stirring for 120 min. Once the time had elapsed, they were centrifuged at 2500 rpm for 5 min, and the absorbance obtained was measured at a maximum wavelength of the selective dye.

3.5.3. Kinetics experiments

For the kinetics experiments, 400 mL of a 30 mg/L solution of the dye was prepared, and 666 mg of adsorbent was added. The solution was adjusted to the optimum pH condition (determined in the test of pH effect) and kept under constant stirring for the established time. Samples were collected every 15 min and measured with the spectrophotometer.

Kinetics analysis was conducted using the common pseudo-1st-order (**Eq. 7**) and pseudo-2nd-order models (**Eq. 8**).

$$q_t = q_e(1 - e^{-k_1 t}) \quad \textbf{(Eq. 7)}$$

$$q_t = \frac{k_2 q_e^2 t}{1 + k_2 q_e t} \quad \textbf{(Eq. 8)}$$

Where $\mathbf{q_e}$ is adsorption capacity at the equilibrium condition (mg/g), **t** is time (min) $\mathbf{k_1}$ is the pseudo-1st-order constant (min^{-1}), and $\mathbf{k_2}$ is the pseudo-2nd-order constant (g/mg min).

3.5.4. Adsorption isotherm

The adsorption isotherm experiments were carried out under optimum pH and contact time conditions and by varying the dye solution's initial concentration. The isotherm of MB adsorption was fitted against the Langmuir (**Eq. 9**) and Freundlich model (**Eq. 10**).

$$q_e = \frac{q_m K_L C_e}{(1 + K_L C_e)} \quad \textbf{(Eq. 9)}$$

$$q_e = K_F C_e^{1/n} \quad \textbf{(Eq. 10)}$$

Where $\boldsymbol{q_m}$ is the maximum adsorption capacity (mg/g), ***b*** is the Langmuir´s constant (L/mg), $\boldsymbol{K_F}$ is the Freundlich adsorption constant (mg/g), and ***n*** is the adsorption affinity (dimensionless).

3.5.5. Adsorption-desorption cycles

After dye adsorption, the recovered adsorbent was washed with ethanol to remove the adsorbed dye and then dried. The collected MOFs were reused for another adsorption cycle. Four cycles were conducted to evaluate the regeneration capability of the MOFs.

3.6. **Chemical waste management**

Waste disposal was followed by the protocols established at the Facultad de Ciencias Químicas.

Table 5. Waste disposal.

Waste	Container
Extractions (Aqueous solution)	A
Methanol, Ethyl acetate	C
Br_2 in HOAc solution	D
Activated carbon with organic compounds	G
MB, IB and MO solution	Colorants and Lugol

CHAPTER 4 RESULTS AND DISCUSSION

4.1. **Synthesis and characterization of compounds 2-5**

All the reactions were monitored by thin-layer chromatography (**Figure 10**), using Hex:EtOAc (1:1) v/v. White powder solids were obtained for all the products. For structural elucidation, the FTIR spectrum (**Figure 11**) shows the characteristic bands of the compounds. As seen, a slight shift in the absorption bands was observed. The characteristic band of the N-H stretch appeared at 3100 cm^{-1}, and the signal at 1667 cm^{-1} was expected to be a C=N stretch. Bands at 1575 and 1052 cm^{-1} are related to the C=C and C-N stretch. Physical properties like melting point and exact mass, summarized in **Table 6**, were also determined to confirm the desired products.

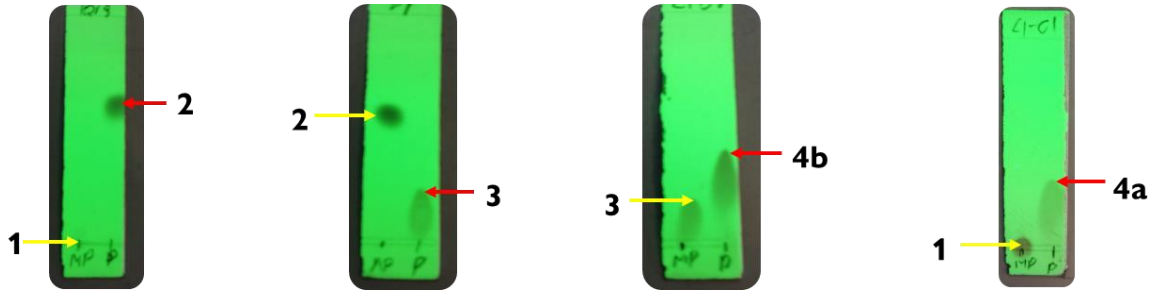

Figure 10. TLC plates of all compounds.

Table 6. *Physicochemical properties of compounds.*

Compound	**Appearance**	**M. P. exp (°C)**	**M. P. rep (°C)**	**E. M. exp (m/z)**	**E.M. calc (m/z)**	**Rf**	**Yield (%)**
2	White powder	219-221	217-220	302.77161	302.77681	0.65	70
3	White powder	126-129	126-132	146.95540	146.95579	0.15	60
4	White powder	198-200	N. R.	180.91651	180.91681	0.26	68
5	White powder	177-180	179-182	136.96571	136.96780	0.20	67

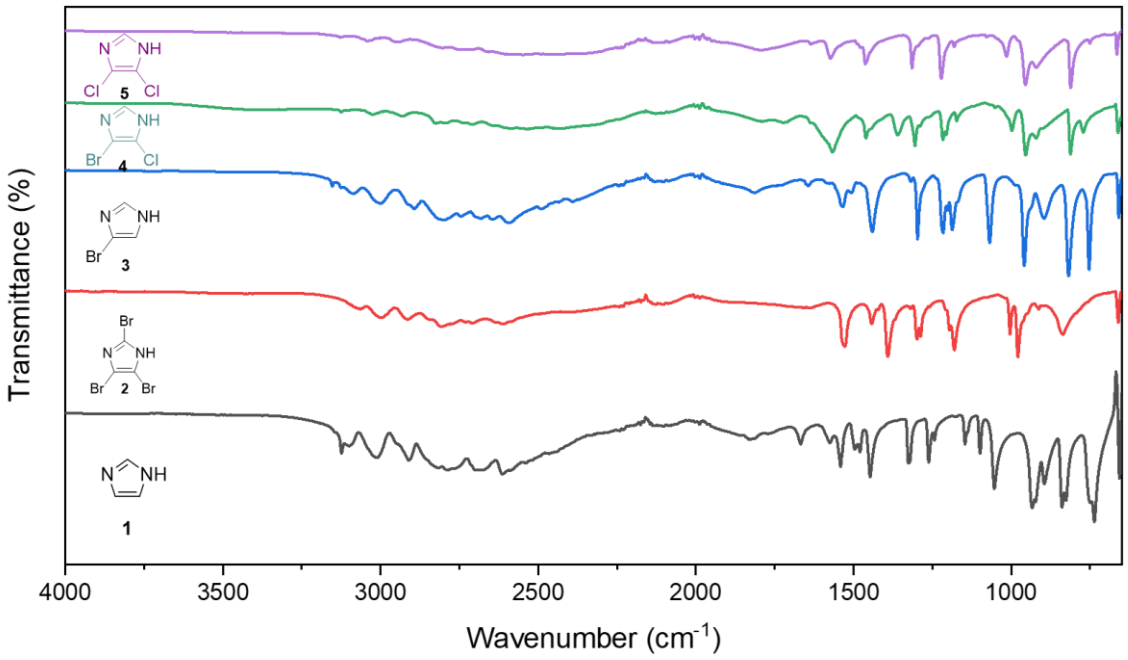

Figure 11. FTIR spectra of compounds **1**, **2**, **3**, **4**, and **5**.

4.2. **Synthesis and characterization of MOFs**

The reactions were monitored by thin-layer chromatography using Hex:EtOAc (1:1) v/v and revealed under UV light. Purple and dark-purple powder solids were obtained. The functional groups of MOFs **Co-Cl** and **Co-Br** were identified by FTIR analysis (**Figure 12**). Neither MOF exhibited a stretching band of N-H, indicating that the reaction proceeded as expected. Furthermore, an intense band from C-N bond absorption appeared at 1035 cm^{-1}, and the 1194-1225 cm^{-1} band corresponded to the imidazolate ring´s in-plane bending. The medium band at 663 cm^{-1} corresponded to the out-of-plane ring deformation.

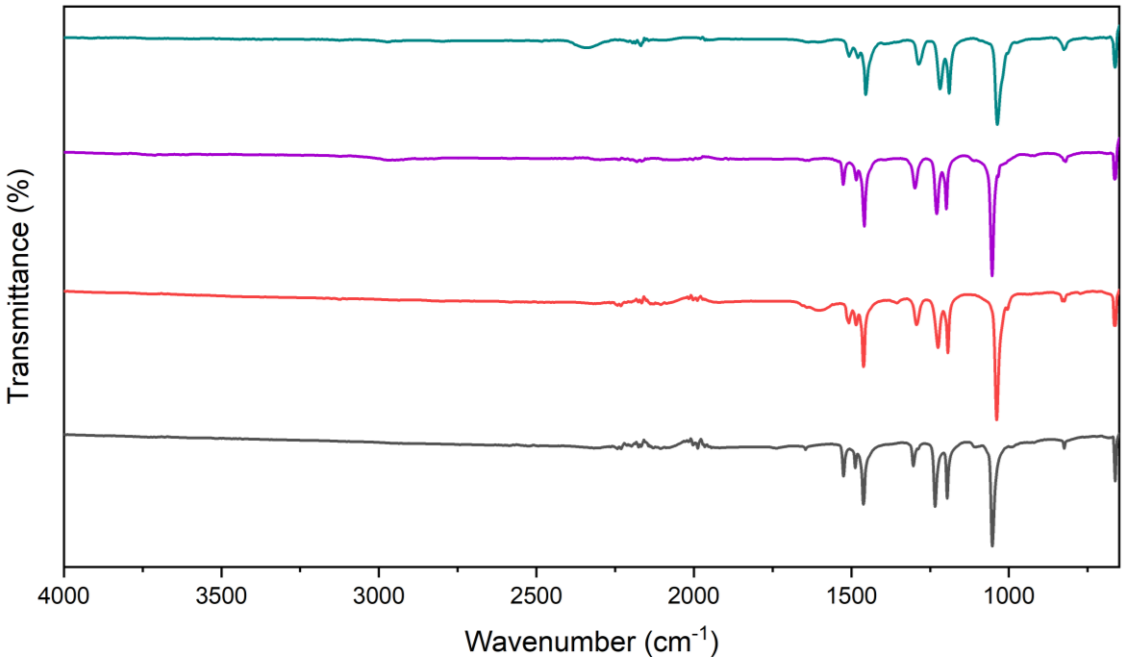

Figure 12. FTIR spectra of **ZIF-71** (black), **ZIF-71(ClBr)** (red), **Co-Cl** (purple), and **Co-Br** (green).

Powder XRD studies (**Figure 13**) were performed on each sample, and the representative pattern on both **Co-Cl** and **Co-Br** showed the characteristic signals of **ZIF-71** (data collected from the Cambridge Crystallographic Data Centre (68)). The diffraction peaks at 2θ= 4.4°, 6.3°, and 7.5° represented the (001), (002), and (112) planes of **ZIF-71**. No additional peaks were detected for **Co-Cl** and **Co-Br**, as reported in the literature (17).

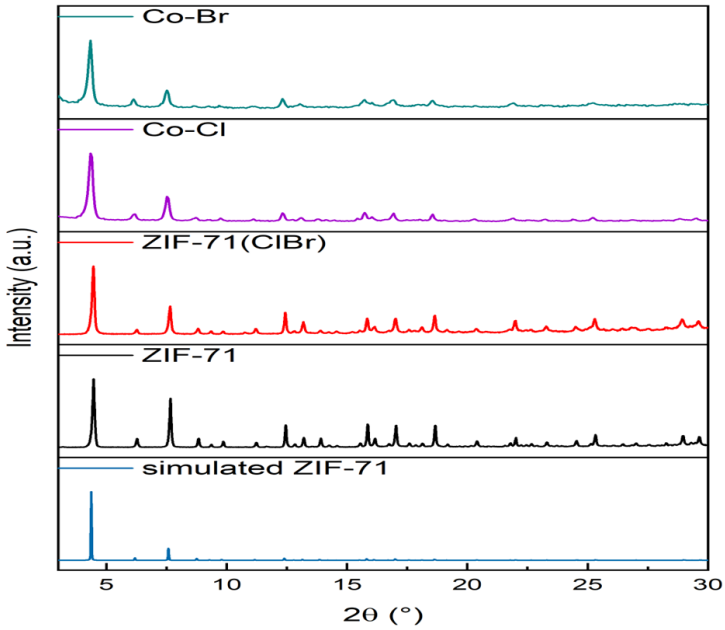

Figure 13. XRD pattern of simulated **ZIF-71** (blue) **ZIF-71**(black), **ZIF-71(ClBr)** (red), **Co-Cl** (purple), and **Co-Br** (green).

To further evaluate the sorption properties of MOFs, nitrogen physisorption was analyzed. The results indicated a typical Type I isotherm (**Figure 14**), as classified by IUPAC (60,69), which corresponds to microporous materials like **ZIF-71**. The surface area (SA) was determined by applying the BET method according to the Rouquerol criteria. **Co-Cl** and **Co-Br** exhibited 900 m^2/g and 700 m^2/g, respectively, consistent with the values previously reported for **ZIF-71** and **ZIF-71(ClBr)** (16).

The determination of the average pore size showed that **Co-Cl** and **Co-Br** have similar pore sizes of 2.85 nm and 2.97 nm. **Co-Cl** exhibits a predominantly microporous structure, as evidenced by the sharp peak below 2 nm. The negligible contribution of mesopores suggest a more uniform pore system. In contrast, **Co-Br** displays a more heterogeneous pore size distribution. While it also possesses micropores, the distribution shows a broader range of mesopores, particularly a significant contribution around 20-40 nm.

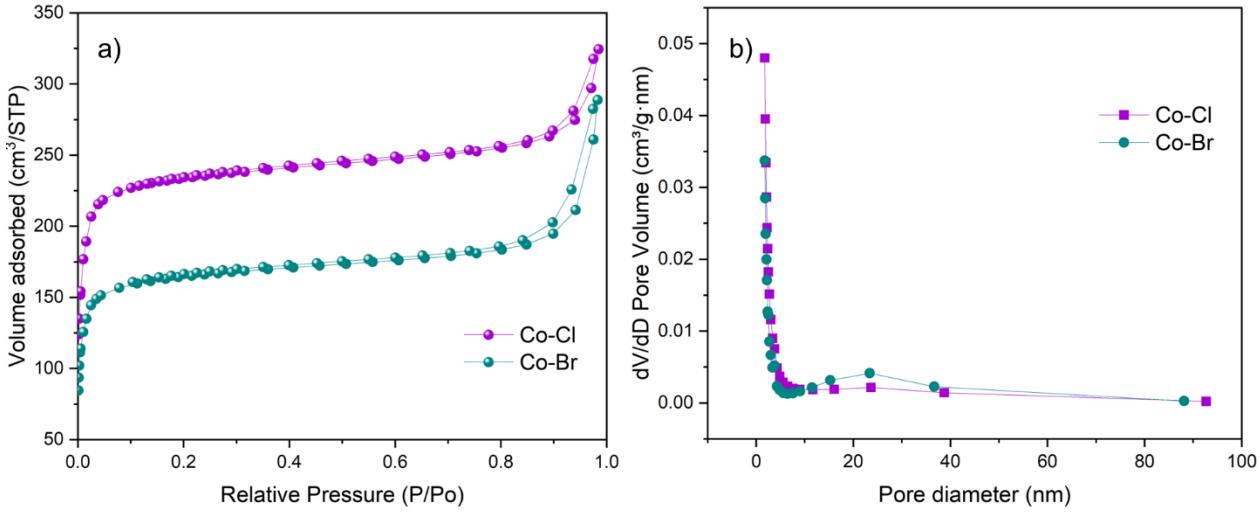

Figure 14. N_2 physisorption a) isotherms and b) pore size distribution of **Co-Cl** and **Co-Br**.

The hydrophobicity of MOFs was evaluated by the static water contact angle (θ) analysis (**Figure 15**). **Co-Cl** (θ= 60.48°) and **Co-Br** (θ= 75.09°) showed favorable wetting, which is regarded as hydrophilic material according to the reported classification. These values indicate lower hydrophobicity compared to **ZIF-8** (98°) (21), **ZIF-71** (107°) (16) and **ZIF-71(ClBr)** (130°) (17). However, **Co-Cl** and **Co-Br** are more hydrophobic than **ZIF-67** (57°) (21) and commercial AC (40°) (70).

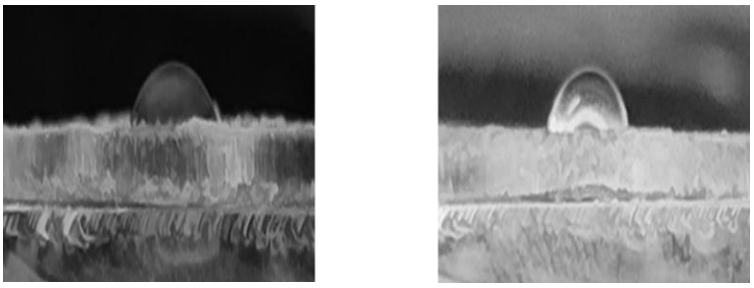

Figure 15. The water contact angle of **Co-Cl** (60°) and **Co-Br (**75°).

Additionally, the point of zero charge (PZC) of **Co-Cl** and **Co-Br** was determined by the salt addition method utilizing NaCl 0.1 M solutions (**Figure 16**). According to the intercept point of the x-axis, the mean values of 3 replicates were 8.4 ± 0.1 for **Co-Cl** and 7.9 ± 0.1 for **Co-Br**. For comparison, the reported PZC of ZIF-67 is approximately 8.7, which is slightly higher than the values obtained for **Co-Cl** and **Co-Br**. This implies that, at a given pH above their respective PZC, **Co-Cl** and **Co-Br** would acquire a more negatively charged surface than **ZIF-67**. Such a condition

could favor the adsorption of cationic dyes due to stronger electrostatic interactions. On the other hand, for anionic dyes, the lower PZC of **Co-Cl** and **Co-Br** may lead to reduced adsorption capacity under acidic to neutral pH conditions compared to **ZIF-67**.

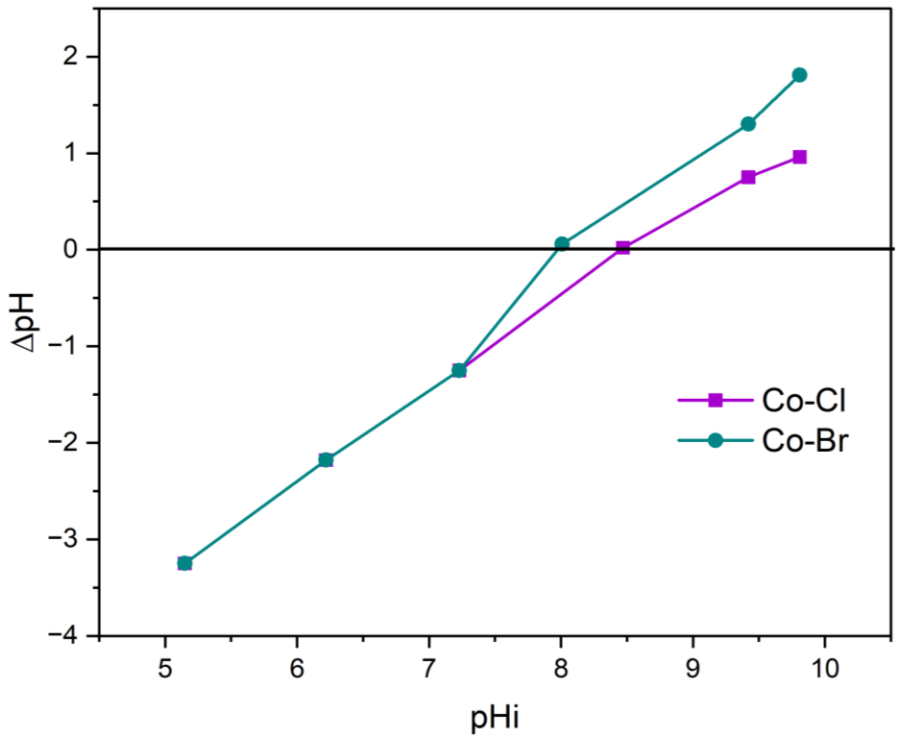

Figure 16. PZC of **Co-Cl** and **Co-Br**.

4.3. **Adsorption studies**

4.3.1. Methylene blue

4.3.1.1. *Effect of pH*

The adsorption capacity was tested at different pH ranges from 4 to 10. **Figure 17** shows similar behavior as the adsorption capacity on MB increased as the pH increased from 4 to 10 on both ZIFs, indicating that MB adsorption is more effective at alkaline conditions. As reported in previous studies (71,72), cationic dyes like methylene blue tend to be adsorbed more effectively at high pH values, similar to the observed behavior. This trend can be explained by the *pKa* value of MB, which is 3.8, meaning that at pH levels above 3.8, the cationic form of the dye predominates, thus enhancing the adsorption of the dye.

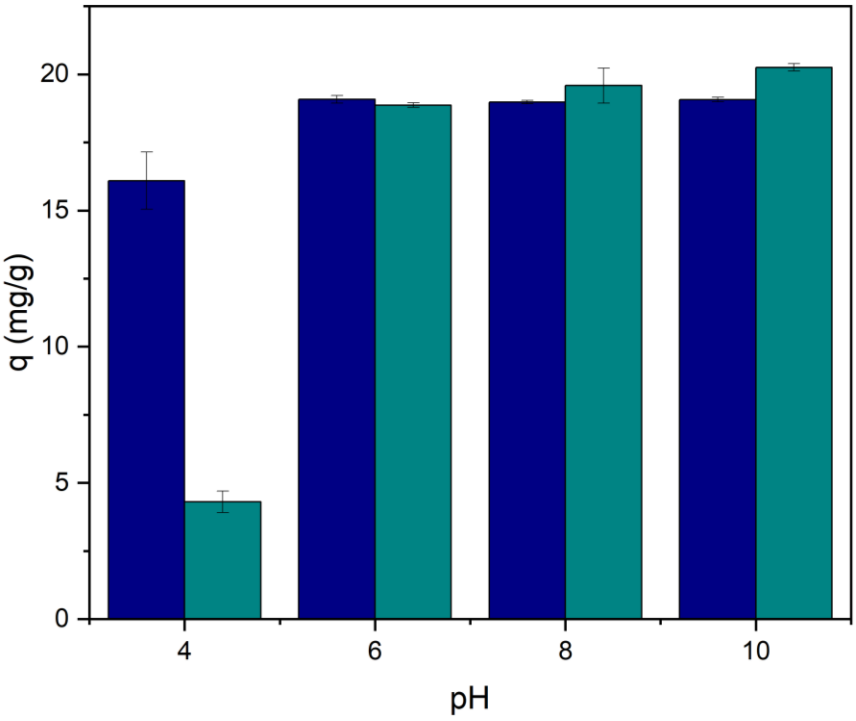

Figure 17. Effect of pH on MB adsorption in **Co-Cl** (blue) and **Co-Br** (green). (Conditions: m= 0.05 g, C_o= 30 mg/L, V= 30 mL, t= 120 min, T= 25 °C)

As a result, the adsorption on MB in both MOFs is not significantly affected in the pH range of 6-10, with an adsorption capacity of 19.01 mg/g and 19.08 mg/g for **Co-Cl** and **Co-Br**, respectively. As established before, the ionic form of the dye predominates in the range of 6-10. Therefore, enhanced adsorption occurs due to non-electrostatic interactions, including Van der Waals forces and *π-π* stacking. In

contrast, when pH is 4, the ionic form of the dye is less, and other interactions are taking place as hydrogen bonds with the MB molecules.

The PZC values of **Co-Cl** (8.4) and **Co-Br** (7.9) provide insight into the behavior observed across this pH range. When the pH is between 4 and 6, the surface charge of the MOFs is positive, causing electrostatic repulsion between the positively charged methylene blue molecules. In contrast, when the pH is between 8-10, enhanced adsorption occurs due to the MOFs' negative surface charge, which leads to electrostatic attraction with the methylene blue molecules.

4.3.1.2. *Kinetics studies*

Kinetic experiments were carried out to evaluate the adsorption of both MOFs further. As shown in **Figure 18**, the decay of methylene blue concentration increases over time. Within the first 15 minutes, 58.44% of MB was removed by **Co-Cl**, whereas 68.50% by **Co-Br**. Both ZIFs reached equilibrium at 60 min, indicating the fast adsorption kinetics on MB. In addition, at equilibrium, the adsorption capacity was 19.01 mg/g (99.19%) and 19.08 mg/g (99.29%) for **Co-Cl** and **Co-Br**, respectively.

The molecular size of MB (1.38 nm x 0.64 nm) (73) is smaller than the pore size of **Co-Cl** (2.84 nm) and **Co-Br** (3.57 nm). In this sense, fast adsorption happens thanks to the available sorption sites on the MOFs' surface. Both MOFs' large surface area and high pore sizes enhanced the adsorption of MB dye.

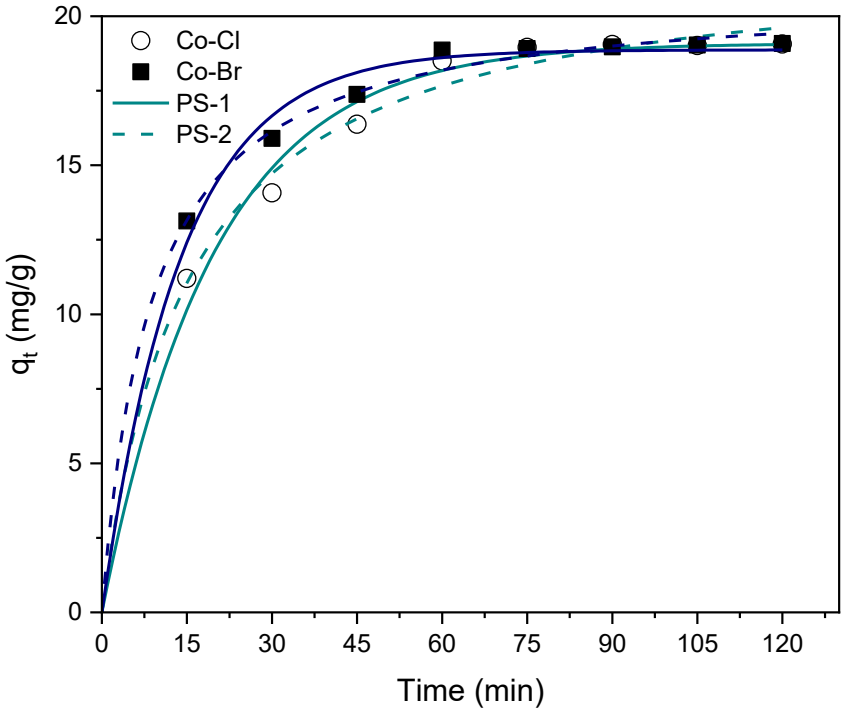

Figure 18. Kinetics of MB adsorption on **Co-Cl** and **Co-Br**. (Conditions: m= 0.666 g, C_o= 30 mg/L, V= 400 mL, pH= 6, T= 25 °C)

The data was fitted against pseudo-1st-order (PS-1) and pseudo-2nd-order (PS-2) kinetic models (**Table 7**). According to the literature, PS-1 states that the main adsorption mechanism is physisorption, which involves the adsorbate interacting on the adsorbent´s surface. In contrast, PS-2 is based on adsorption, called chemisorption, which refers to the interaction between adsorbate and adsorbent due to the formation of solid bonds. In this framework, the adsorption onto both MOFs fitted well against the PS-2 model as indicated by the correlation coefficient. In addition, both models' calculated adsorption capacities at equilibrium (q_e) were very close to the experimental values.

Table 7. Kinetic parameters of MB adsorption on **Co-Cl** and **Co-Br**.

Adsorbent	qe_{exp} (mg/g)	PS-1			PS-2		
		qe_{calc} (mg/g)	k_1 (min^{-1})	r^2	qe_{calc} (mg/g)	k_2 (g mg^{-1} min^{-1})	r^2
Co-Cl	19.15	19.09	0.0505	0.9506	22.06	0.0030	0.9635
Co-Br	19.08	18.87	0.0714	0.9346	20.84	0.0054	0.9733

4.3.1.3. Adsorption isotherm

The adsorption isotherms (**Figure 19**) were fitted against the Langmuir and Freundlich models to identify the distribution of the adsorbed molecules between liquid and solid phases when the adsorption reaches an equilibrium state. **Co-Cl** is fitted well with the Freundlich model, whereas **Co-Br** is fitted well with the Langmuir model according to the correlation coefficient value (r^2) (**Table 8**). Freundlich states that adsorption occurs on a heterogeneous surface, meaning that not all sorption sites have the same affinity. Meanwhile, the Langmuir model is based on adsorption on a homogenous surface, meaning that all sorption sites have the same affinity. The q_m of **Co-Cl** is greater than that of **Co-Br**, suggesting that the difference in surface area is the main cause. Despite **Co-Br** having a higher pore size than **Co-Cl**, the surface area seems to be a more critical parameter, affecting the dye adsorption. Experimentally, the q_m was 119.21 mg/g and 61.42 mg/g for **Co-Cl** and **Co-Br**, which are close to the theoretical values of the models.

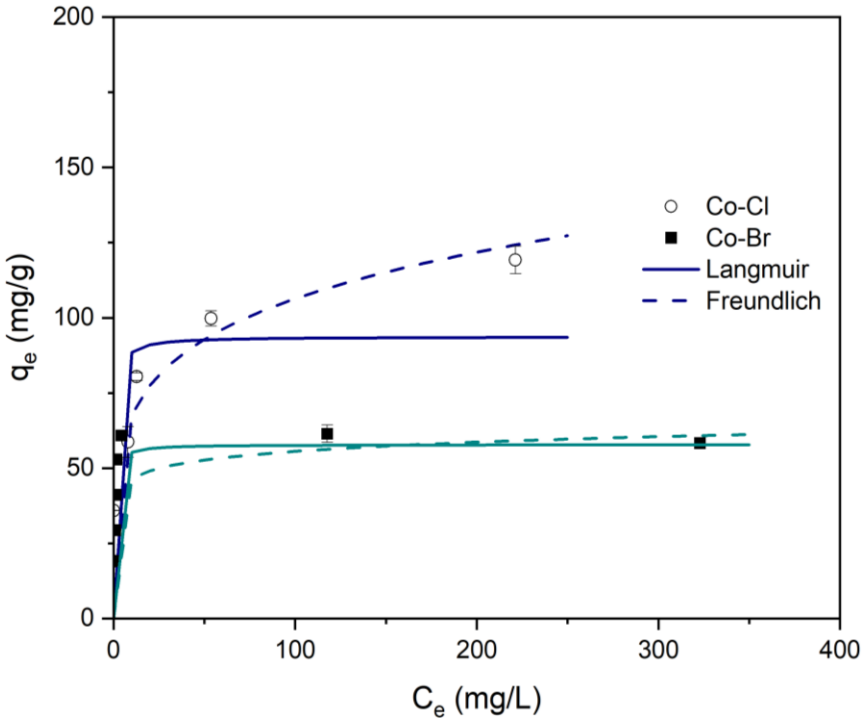

Figure 19. Adsorption isotherms of MB on **Co-Cl** and **Co-Br**. (Conditions: m= 0.05 g, V= 30 mL, pH= 6, t= 60 min, T= 25 °C)

Table 8. Isotherm models parameters of MB adsorption on **Co-Cl** and **Co-Br**.

Adsorbent	Langmuir			Freundlich		
	q_m (mg/g)	K_L (L/mg)	r^2	K_F (L/g)	n	r^2
Co-Cl	93.71	1.70	0.6921	43.05	5.09	0.9425
Co-Br	57.83	2.15	0.9362	38.97	12.97	0.8294

4.3.1.4. Adsorption-desorption cycles

After adsorption, the recovered adsorbents were washed with ethanol to remove the adsorbed dye and dried. The recollected ZIFs were then reused for additional dye adsorption, and four cycles were performed for both adsorbents. As shown in **Figure 20**, the removal of methylene blue decreases as both ZIFs were reused over multiple cycles. The adsorption of methylene blue remained above 80% after three cycles but then decreased to 56% for **Co-Cl**. Nevertheless, **Co-Br** performs better, maintaining a high removal percentage above 85% after all four cycles. The hydrophobic nature of **Co-Br** enhanced its stability in aqueous solutions, reducing its interactions with water molecules and thereby providing more available sorption sites.

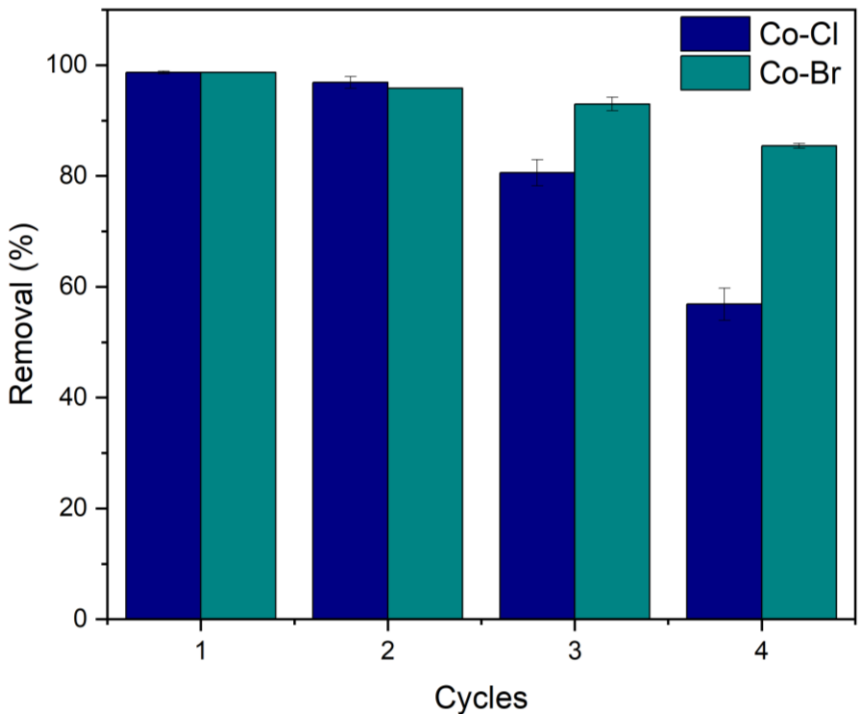

Figure 20. Cycles of adsorption of MB on **Co-Cl** and **Co-Br**. (Conditions: m= 0.05 g, V= 30 mL, Solvent= EtOH, t= 60 min, T= 25 °C)

Moreover, the decrease in adsorption performance, particularly in the case of **Co-Cl**, may also be attributed to non-electrostatic interactions between dye molecules and the active sites of the MOFs, which could lead to stronger binding and partial blockage of sorption sites over successive cycles, thus limiting the regeneration efficiency of the material. To confirm this assumption, FTIR analysis was performed on the loaded MOFs after the final cycle. As shown in **Figure 21**, the appearance of the stretching band at 1600 cm^{-1} of C=N and 882-838 cm^{-1} of C-S-C corresponds to the thiazine group of the MB.

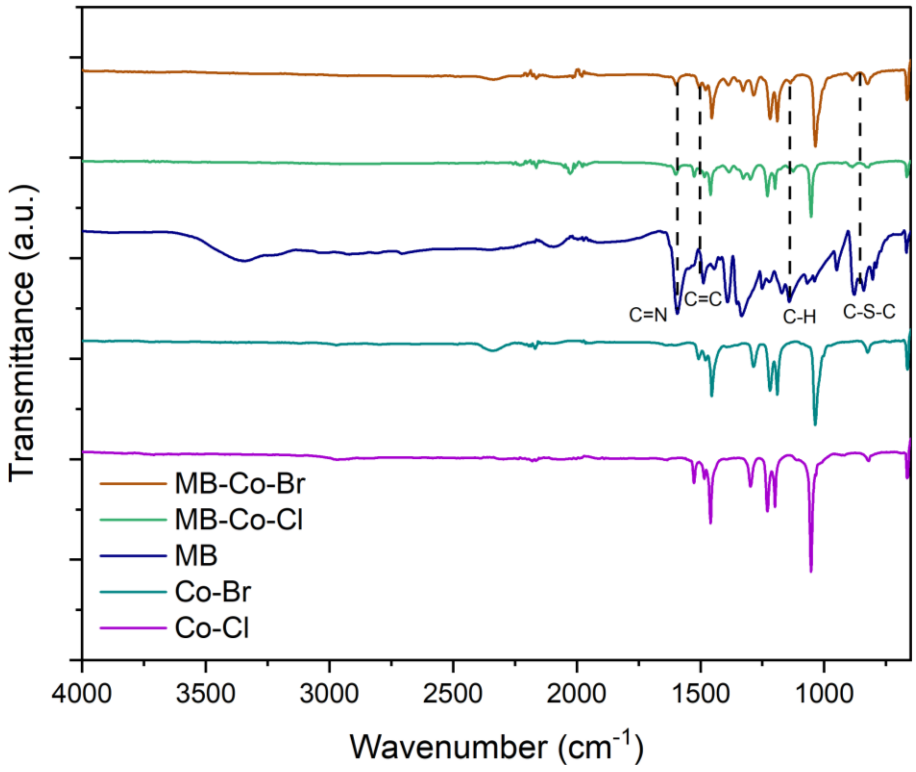

Figure 21. FTIR of **Co-Cl** (purple), **Co-Br** (green), MB (blue), loaded MB on **Co-Cl** (dark green), and **Co-Br** (brown).

4.3.1.5. Comparison with other adsorbents

The q_m values for **Co-Cl** and **Co-Br** highlight their potential against other common adsorbents summarized in **Table 9**. Both MOFs present better adsorption performance than most used MOFs like ZIFs, UiO-66, and MIL derivatives. In addition, these MOFs present better adsorption capacities than other activated carbons derived from different waste sources. Fast adsorption kinetics and high adsorption capacities revealed the potential of these adsorbents for future industrial applications.

Table 9. Adsorbents used for MB adsorption.

Material	q_m (mg/g)	Reference
ZIF-8	57.14	(20)
ZIF-67	24.57	(25)
Cu-BTC	39.5	(74)
Co-doped Fe BDC	23.92	(75)
UiO-66	13.11	
UiO-67	54.81	(76)
MIL-100(Fe)	52.11	
Ball mill AC	50.27	(77)
AC from sugarcane	51.00	(23)
Co-Cl	93.71	This work
Co-Br	57.83	

4.3.2. Methyl orange

4.3.2.1. Effect of pH

According to **Figure 22**, pH is an essential factor in the adsorption of methyl orange. The adsorption capacity of the MOFs increases as pH decreases. When the pH is 4, the adsorption capacity for **Co-Cl** and **Co-Br** was 12.61 mg/g and 11.80 mg/g, respectively. On the other hand, more alkaline conditions, like pH 6, 8, and 10, lead to a decrease of 10.69 mg/g and 2.62 mg/g for **Co-Cl** and **Co-Br**.

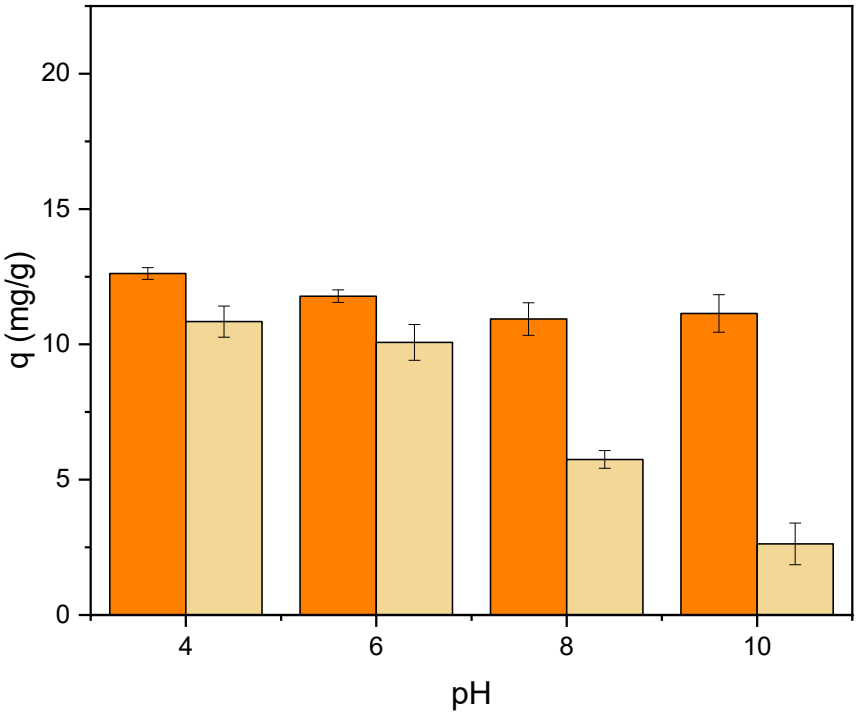

Figure 22. Effect of pH on MO adsorption in **Co-Cl** (orange) and **Co-Br** (cream). (Conditions: m= 0.05 g, C_o= 30 mg/L, V= 30 mL, t= 120 min, T= 25 °C)

Methyl orange is a molecule with a negative charge under acidic conditions (*pKa* = 3.4). When the pH is around 4 (close to the pKa value of MO), approximately 50% of the MO molecules are in their neutral form, allowing *π-π* interactions between the aromatic ring of the MO molecule and the imidazolate linker of **Co-Cl** and **Co-Br**, which enhances MO adsorption. On the contrary, at pH > 6, the dye's ionic form predominates; still, the -OH concentration gradually increases and competes with the dye molecules for the available sorption sites of the MOFs, decreasing adsorption capacity.

Moreover, the pzc values for **Co-Cl** and **Co-Br** help explain the observed behavior within this pH range. When the pH is between 4 and 6, the MOFs exhibit a positive surface charge, resulting in electrostatic attraction with the negatively charged methyl orange molecules and, thus, enhancing the adsorption onto methyl orange. In contrast, at a pH range of 8 to 10, the MOFs have a negative surface charge, reducing the adsorption through electrostatic repulsion with methyl orange.

4.3.2.2. Kinetics studies

According to the graph shown in **Figure 23**, methyl orange concentration decreases over time. During the first 15 minutes of adsorption, **Co-Br** removed 37% (6.92 mg/g) of the initial dye concentration, meanwhile, **Co-Cl** adsorbed 5% (1.15 mg/g). For **Co-Cl** there was not observed equilibrium condition during the established time of 120 min, therefore, the adsorption time was extended to 180 min. In this sense, **Co-Br** reached equilibrium condition at 75 min, whereas **Co-Cl** at 150 min. Moreover, the adsorption capacity at equilibrium time was 19 mg/g and 10.50 mg/g for **Co-Cl** and **Co-Br**, respectively.

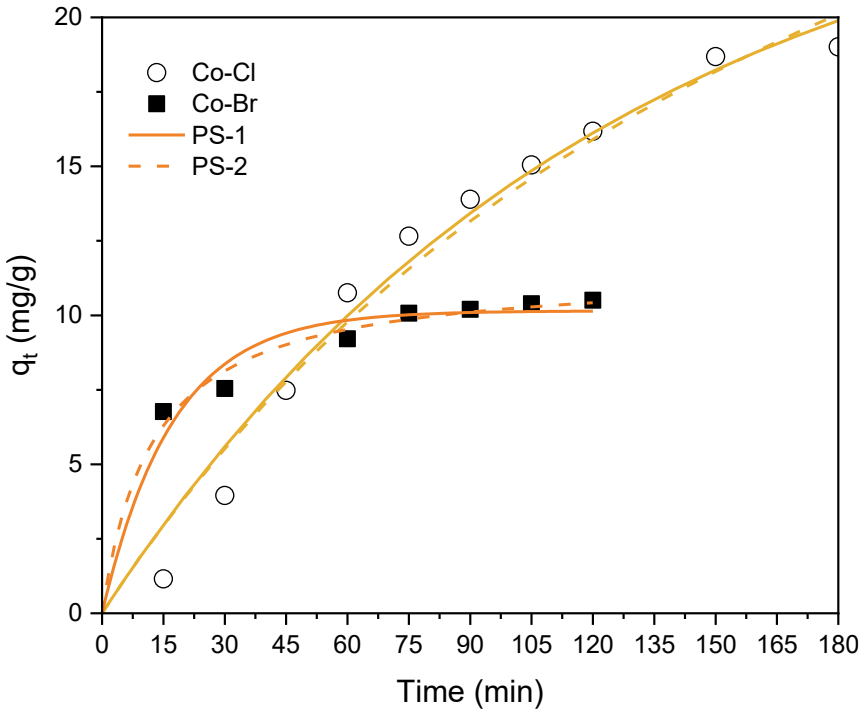

Figure 23. Kinetics of MO adsorption on **Co-Cl** and **Co-Br**. (Conditions: m= 0.666 g, C_o= 30 mg/L, V= 400 mL, pH= 4, t= 150 min, T= 25 °C)

The pore size of the MOFs can affect the adsorption of methyl orange. **Co-Br** exhibits a higher pore size (3.57 nm) than **Co-Cl** (2.84 nm) facilitating the diffusion of MO molecules (1.31 nm x 0.55 nm) (73) into the pores of **Co-Br**. Besides, the enhanced hydrophobic property of **Co-Br** enhances the interaction between the MO molecules and decreases non-desirable interactions with water molecules. As a result, the adsorption of MO on **Co-Br** is faster than in **Co-Cl**.

The data was fitted with PS-1 and PS-2 kinetic models. Both MOFs fit well with the PS-2 model, as indicated by the correlation coefficient (**Table 10**). These results further indicate that the PS-2 model is more suitable for the adsorption of MO on the MOFs´ external surface. Moreover, the experimental and calculated q_e values show good agreement.

Table 10. Kinetic parameters of MO adsorption on **Co-Cl** and **Co-Br**.

Adsorbent	qe_{exp} (mg/g)	PS-1			PS-2		
		qe_{calc} (mg/g)	k_1 (min^{-1})	r^2	qe_{calc} (mg/g)	k_2 (g mg^{-1} min^{-1})	r^2
Co-Cl	19.00	25.89	0.0081	0.9701	42.52	0.0001	0.9651
Co-Br	10.51	10.14	0.0579	0.9954	11.49	0.0070	0.9912

4.3.2.3. Adsorption isotherm

To further evaluate the adsorption of MO on **Co-Cl** and **Co-Br**, isotherm analysis was employed. The data were fitted according to the common isotherm models of Langmuir and Freundlich. The correlation coefficient indicates that **Co-Cl** and **Co-Br** fit well with the Freundlich model, suggesting multilayer adsorption on heterogeneous surfaces.

However, it is important to note that these results may not accurately represent the true maximum adsorption capacity of the MOFs due to the experimental conditions. At high methyl orange concentrations (> 150 mg/L) and pH 4, precipitation occurs, which interferes with the adsorption measurements. This precipitation introduces uncertainty in determining the actual equilibrium concentration of the solution, thereby affecting the accuracy of the adsorption isotherms.

For this reason, experiments were not continued at higher concentration levels, as the precipitated dye would make it difficult to distinguish between adsorption onto the MOF and simple phase separation. To ensure reliable and reproducible results, adsorption studies were limited to concentration ranges where precipitation effects were not observed. As a result, the experimental maximum adsorption capacities determined at these conditions were 265.01 mg/g and 247.25 mg/g for **Co-Cl** and **Co-Br**, respectively.

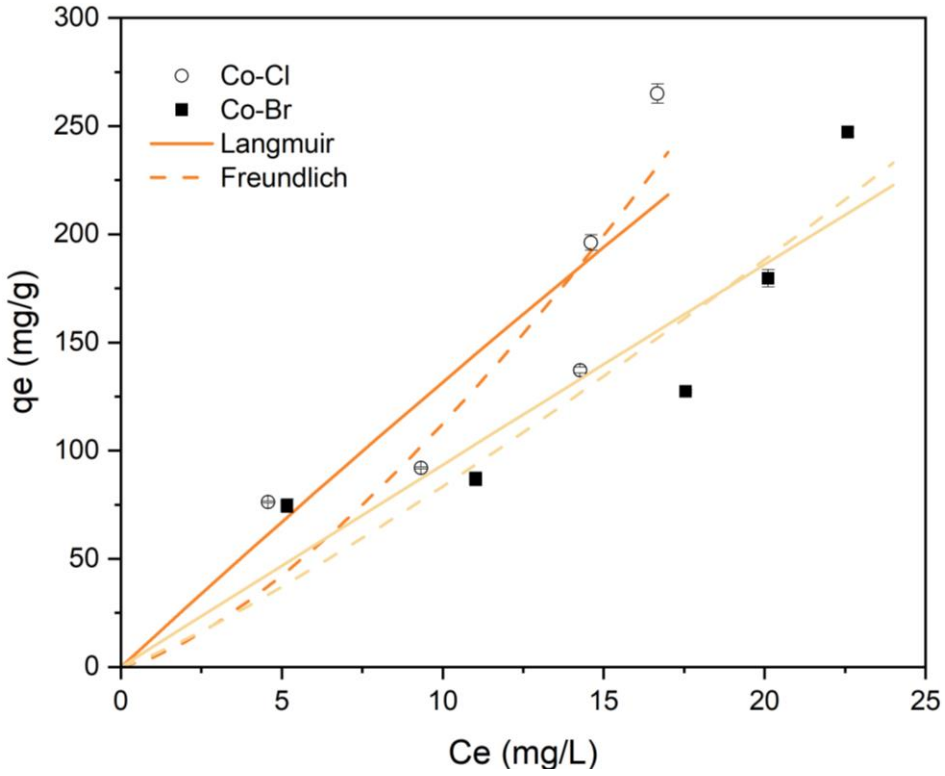

Figure 24. Adsorption isotherms of MO on **Co-Cl** and **Co-Br**. (Conditions: m= 0.01 g, V= 30 mL, pH= 4, t= 150 min, T= 25 °C)

Table 11. Isotherm models parameters of MO adsorption on **Co-Cl** and **Co-Br**.

Adsorbent	Langmuir			Freundlich		
	q_m (mg/g)	K_L (L/mg)	r^2	K_F (L/g)	n	r^2
Co-Cl	28070.48	4.63×10^{-6}	0.6786	4.34	0.70	0.8697
Co-Br	55927.27	16.86×10^{-6}	0.7588	5.61	0.85	0.7689

4.3.2.4. Adsorption-desorption cycles

An important parameter to evaluate in the adsorption method is the regeneration of the adsorbent used. Therefore, after the adsorption process, the recovered solid was dried and used for another adsorption. After two adsorption processes the removal percentage decreases, 52% and 62% for **Co-Cl** and **Co-Br**, respectively. After the third cycle, only 5% of MO molecules were adsorbed for **Co-Br**, whereas 1.17% for **Co-Cl**. This behavior can be attributed to the difference in the hydrophobic properties of both MOFs. **Co-Cl** (θ= 57°) is less hydrophobic than **Co-Br** (θ= 72°), thus, water molecules can saturate the available sorption sites faster.

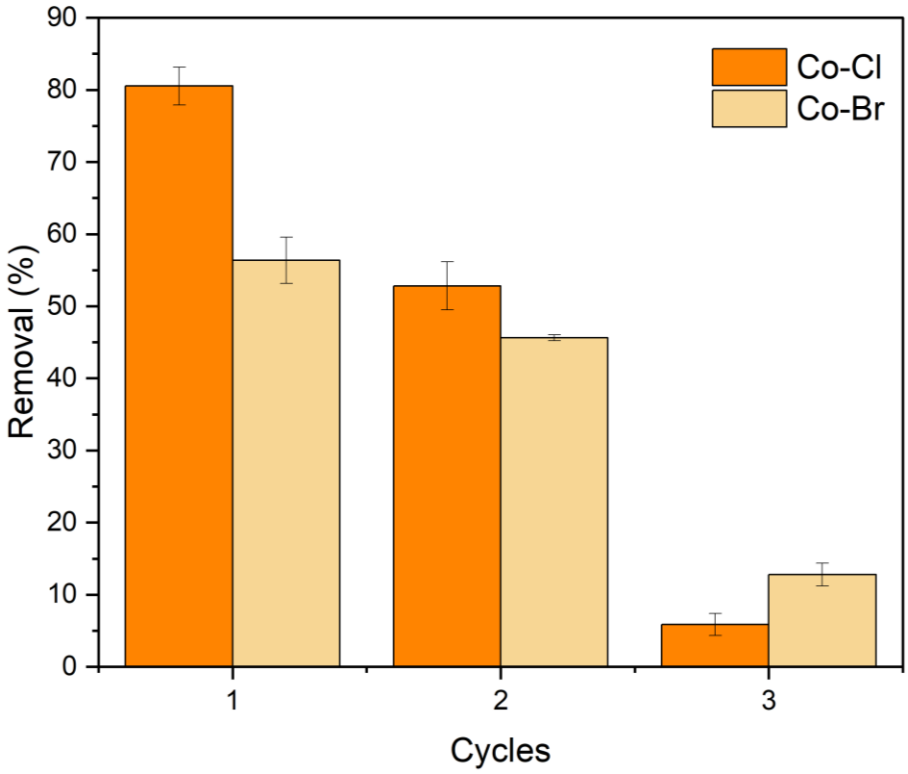

Figure 25. Cycles of adsorption of MO on **Co-Cl** and **Co-Br**. (Conditions: m= 0.05 g, V= 30 mL, pH= 4, t= 150 min, T= 25 °C)

Additionally, the progressive reduction in adsorption capacity may also result from strong electrostatic interactions between the anionic methyl orange molecules and the positively charged sites of the MOFs, which could limit the complete desorption during regeneration steps, leading to the accumulation of irreversibly bound dye and a subsequent loss of active sites. This was further supported by the FTIR analysis

(**Figure 26**), which confirmed the presence of characteristic bands corresponding to MO on the regenerated MOFs.

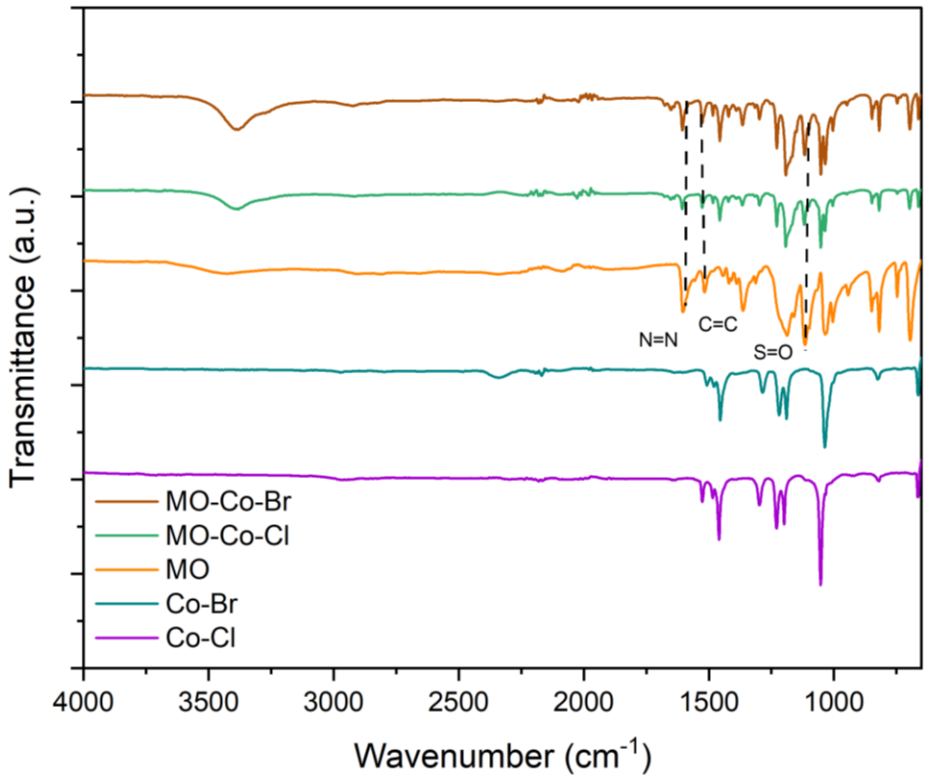

Figure 26. FTIR of **Co-Cl** (purple), **Co-Br** (green), MO (orange), loaded MO on **Co-Cl** (dark green), and **Co-Br** (brown).

4.3.2.5. Comparison with other adsorbents

The outstanding performance of Co-Cl and Co-Br in MO removal is reflected in their high qm values (**Table 12**), which combined with fast adsorption kinetics with remarkable capacities. These properties place them ahead of a variety of conventional adsorbents, including activated carbons from different waste sources. When compared to other widely investigated MOFs, like UiO-66 and MIL-type materials, both Co-based frameworks exhibit clear superiority, emphasizing their strong potential as next generation for large-scale industrial applications where efficiency and speed are critical.

Table 12. Adsorbents used for MO adsorption.

Adsorbent	q_m (mg/g)	Reference
ZIF-8	322.58	(28)
ZIF-67	1342.00	(30)
UiO-66	84.80	(78)
MIL-101(Cr)	196.00	(79)
MIL-53(Al)	100.00	
AC from sugarcane	161.80	(29)
Commercial AC	77.10	
Co-Cl	265.01	This work
Co-Br	247.25	This work

4.3.3. Congo red

4.3.3.1. Effect of pH

The impact of initial solution pH on the adsorption capacity onto the MOFs was analyzed at various levels (pH= 4-10). **Figure 27** shows the effect of pH on the adsorption of MOFs. The highest adsorption capacities of 12.76 mg/g (81%) and 13.83 mg/g (88%) for **Co-Cl** and **Co-Br** were determined at pH=4. As the solution pH increases from 4 to 10, the adsorption capacity decreases achieving values of 6.76 mg/g (43%) and 10.91 mg/g (70%).

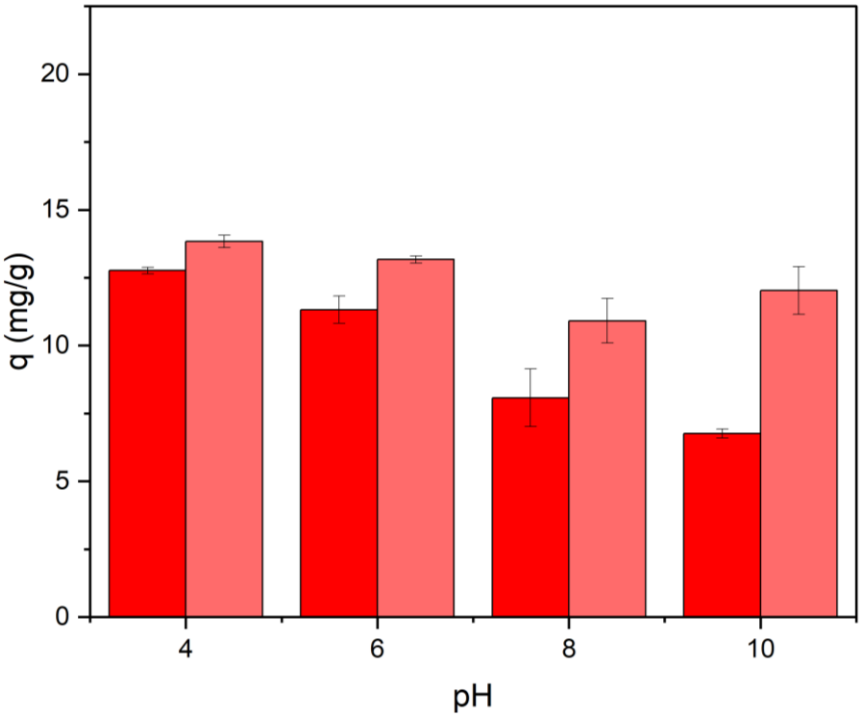

Figure 27. Effect of pH on CR adsorption in **Co-Cl** (red) and **Co-Br** (light red). (Conditions: m= 0.05 g, C_o= 30 mg/L, V= 30 mL, t= 120 min, T= 25 °C)

Since Congo red is a typical anionic dye (*pKa*= 3.9), the degree of ionization is determined by the pH solution. During the whole test, the dye was in its ionic form properly enhancing the electrostatic forces with the adsorbents. However, increasing the pH above 6 decreases the adsorption capacity. This can be attributed to the ^{-}OH ions in the solution may compete with the negative charge of CR molecules when interacting with the positive charge of Co^{2+} of the MOFs. This idea indicates that the adsorption of CR can be affected mainly by electrostatic interactions.

Furthermore, the pzc values help clarify the behavior seen across this pH range. In the pH range of 8 to 10, the MOFs become negatively charged, leading to reduced adsorption due to electrostatic repulsion with Congo red molecules. Conversely, at pH 4 the MOFs present a positive charge, which promotes adsorption of Congo red by facilitating electrostatic attractions with its negatively charged molecules. Therefore, pH 4 was maintained for the next experiments.

4.3.3.2. Kinetics studies

To provide new insights into the adsorption of Congo red, kinetic experiments were evaluated from 0 to 120 min. **Figure 28** shows the behavior of adsorption capacity over time. During the first 45 min, the MOFs adsorbed almost all the CR molecules, 66.45% for **Co-Cl** and 67.12% for **Co-Br**. After 60 min, the MOFs reached equilibrium conditions, meaning the CR molecules saturated all available sorption sites. In this sense, the adsorption capacity at equilibrium was 12.15 mg/g and 13.08 mg/g for **Co-Cl** and **Co-Br**, respectively. The molecular size of Congo red (2.6 nm x 0.93 nm) (73) is smaller than the pore size of the MOFs. **Co-Cl** and **Co-Br** exhibit fast adsorption because the diffusion process is facilitated onto the MOFs´ surface.

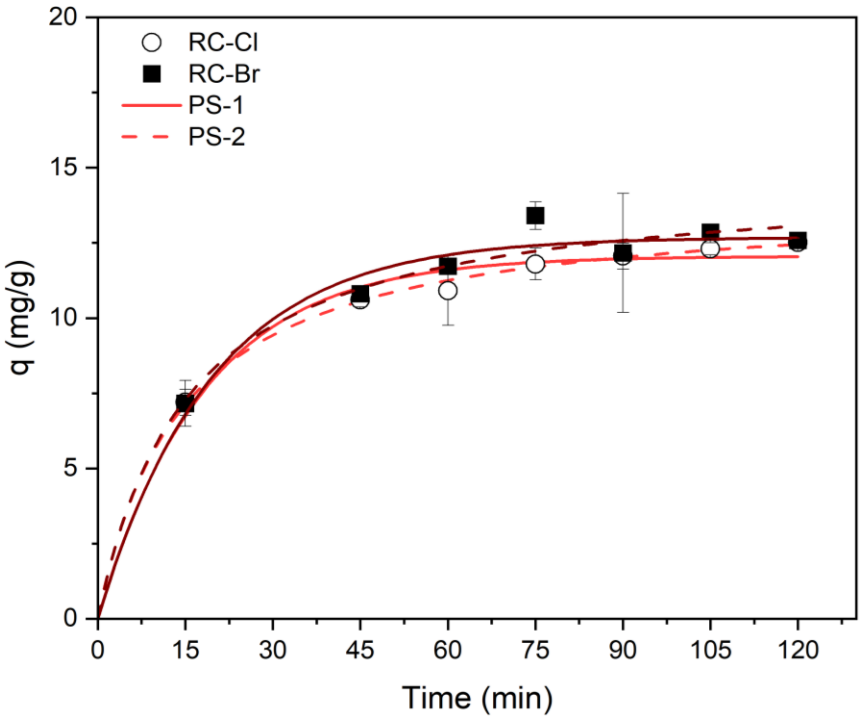

Figure 28. Kinetics of CR adsorption on **Co-Cl** and **Co-Br**. (Conditions: m= 0.666 g, C_o= 30 mg/L, V= 400 mL, pH= 4, T= 25 °C)

Experimental data were analyzed using the PS-1 and PS-2 models to further evaluate the adsorption mechanisms of **Co-Cl** and **Co-Br**. According to the correlation coefficient, the MOFs were adjusted to the PS-2 model. **Table 13** summarizes the kinetic parameters of both MOFs. In addition, the calculated and experimental q_e were very close.

Table 13. Kinetic parameters of CR adsorption on **Co-Cl** and **Co-Br**.

Adsorbent	qe_{exp} (mg/g)	PS-1			PS-2		
		qe_{calc} (mg/g)	k_1 (min^{-1})	r^2	qe_{calc} (mg/g)	k_2 (g mg^{-1} min^{-1})	r^2
Co-Cl	12.15	12.05	0.0545	0.9307	13.93	0.0050	0.9920
Co-Br	13.08	12.68	0.0512	0.9208	14.72	0.0044	0.9212

4.3.3.3. Adsorption isotherm

The adsorption isotherms (**Figure 29**) were analyzed using the Langmuir and Freundlich models to understand the distribution of the adsorbed molecules between liquid and solid phases at equilibrium. The Langmuir model, which assumes a homogeneous surface with uniform sorption site affinity, provided a better fit for **Co-Cl** and **Co-Br** based on the correlation coefficient (r^2) (**Table 14**). The higher adsorption capacity (q_m) of **Co-Br** compared to **Co-Cl** suggests that pore size plays a more crucial role in adsorption than surface area, even though **Co-Br** has a higher surface area. Experimentally, the maximum adsorption capacities were determined to be 1803.37 mg/g and 2100 mg/g for **Co-Cl** and **Co-Br**, aligning closely with the theoretical values predicted by the adsorption models.

Table 14. Isotherm models parameters of CR adsorption on **Co-Cl** and **Co-Br**.

Adsorbent	Langmuir			Freundlich		
	q_m (mg/g)	K_L (L/mg)	r^2	K_F (L/g)	n	r^2
Co-Cl	1852.75	0.20	0.8498	522.85	4.38	0.6383
Co-Br	2240.24	0.08	0.9744	398.07	3.10	0.8484

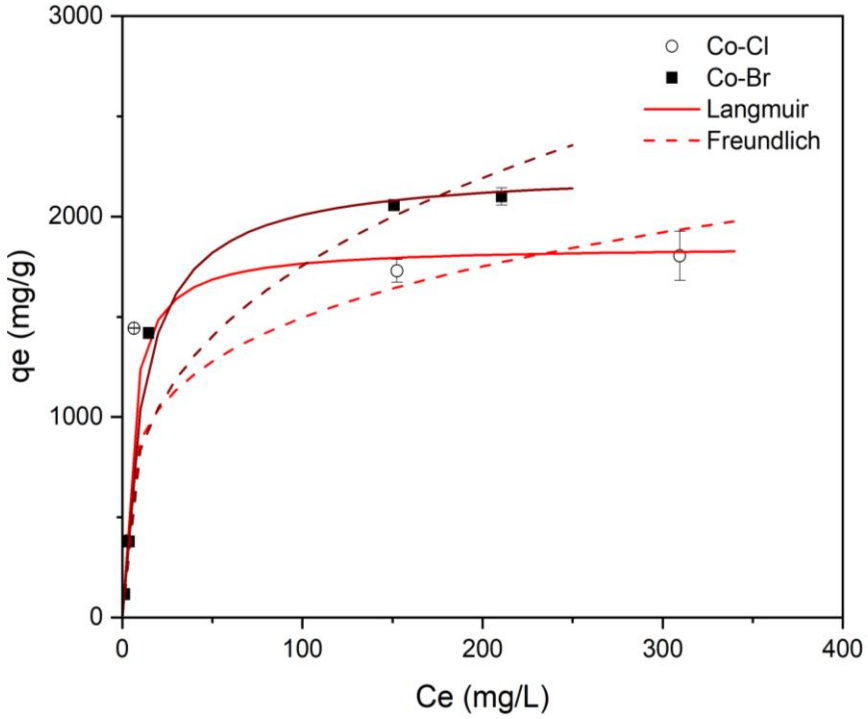

Figure 29. Adsorption isotherms of **Co-Cl** and **Co-Br**. (Conditions: m= 0.01 g, C_o= 30 mg/L, V= 30 mL, pH= 4, t= 60 min, T= 25 °C)

4.3.3.4. Adsorption-desorption cycles

A critical factor in assessing the adsorption method is the regenerability of the adsorbent. After the initial adsorption, the recovered solid was dried and reused for subsequent adsorption cycles (**Figure 30**). After two cycles, the removal efficiency dropped to 50% for **Co-Cl** and 40% for **Co-Br**. By the third cycle, only 15% of CR molecules were adsorbed by **Co-Cl** and 9% by **Co-Br**. Interestingly, **Co-Br** exhibits

lower performance than **Co-Cl** despite presenting a higher hydrophobic property.

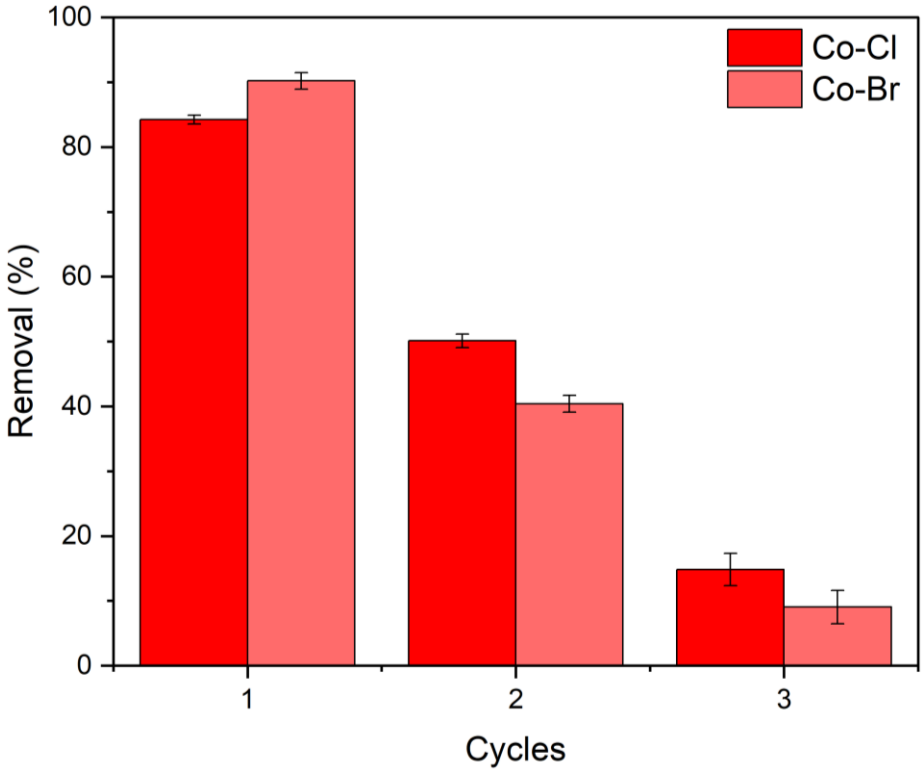

Figure 30. Cycles of adsorption of CR on **Co-Cl** and **Co-Br**. (Conditions: m= 0.05 g, C_o= 30 mg/L, V= 30 mL, t= 60 min, T= 25 °C)

This behavior could be attributed to strong electrostatic interactions between the anionic Congo red molecules and positively charged sites on the MOFs, which may limit dye desorption during regeneration and result in the progressive blockage of active sites. Interestingly, FTIR analysis (**Figure 31**) did not reveal the characteristics bands of CR on the regenerated MOFs, which could be due to either the low amount of dye retained on the surface or overlapping with the framework´s own vibrational modes. Computational studies are required to investigate the nature of this interaction, which falls beyond the scope.

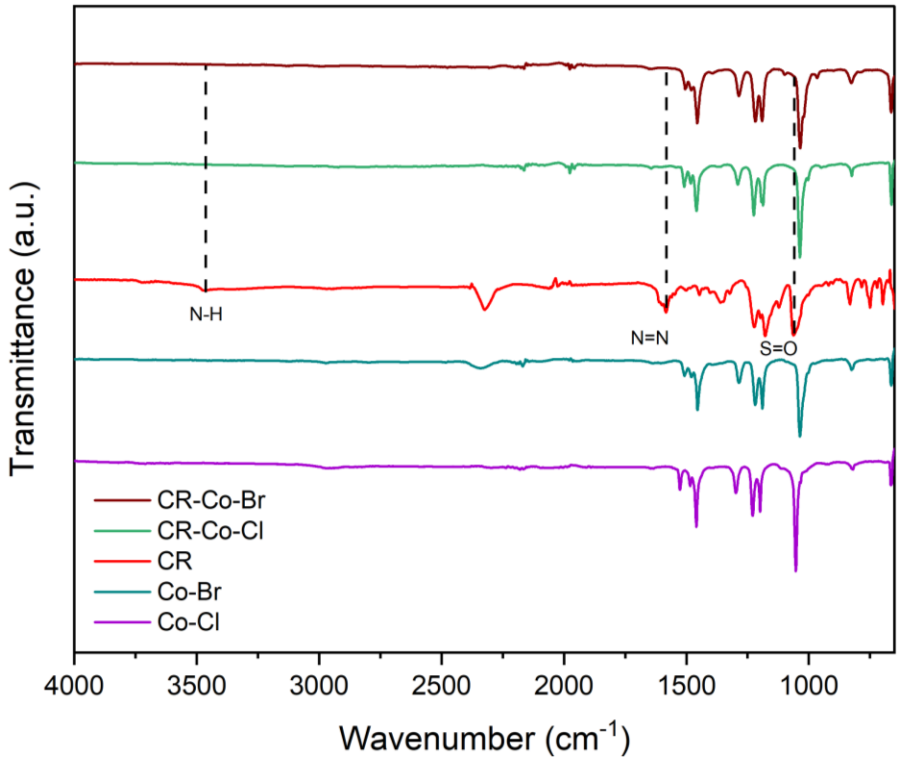

Figure 31. FTIR of **Co-Cl** (purple), **Co-Br** (green), CR (red), loaded CR on **Co-Cl** (dark green), and **Co-Br** (brown).

4.3.3.5. Comparison with other adsorbents

The q_m values for **Co-Cl** and **Co-Br** demonstrate their strong potential compared to other widely used adsorbents (**Table 15**). Both MOFs exhibit superior adsorption performance when compared to commonly studied MOFs, such as ZIFs, UiO-66, and MIL derivatives, which are frequently employed for dye removal. In addition, these MOFs outperform various activated carbons derived from different waste sources. The combination of fast adsorption kinetics and high adsorption capacities highlights the promising application of these materials for future industrial applications, where efficient adsorbents are in high demand.

Table 15. Adsorbents used for CR adsorption.

Material	q_m (mg/g)	Reference
ZIF-8	1250.00	(34)
ZIF-67	714.30	(33)
Cu-BTC	884.96	(80)
UiO-66	623.00	(81)
UiO-67	2360.00	(82)
MIL-100(Fe)	714.00	(83)
AC from Spathodea campanulate flowers	59.27	(84)
AC from Peony seeds shell	2003.20	(85)
Co-Cl	1852.75	This work
Co-Br	2240.24	

4.3.4. Comparison of dyes adsorption

According to the literature, the pK_a of the dyes are around 3.8 for methylene blue, 3.4 for methyl orange, and 4.1 for Congo red. At pH values above the pK_a, the dyes' ionic forms predominate, enhancing adsorption. As reported in previous studies, cationic dyes like MB tend to be adsorbed more effectively at high pH values (X), whereas at low pH values for anionic dyes like MO and CR. This assumption can be attributed to the pzc values of **Co-Cl** and **Co-Br** being 8.4 and 7.9. When the pH>pzc, the surface of the MOFs exhibits a negative charge enhancing adsorption of the cationic dye (MB). Conversely, at pH<pzc, the MOFs are positively charged, thereby enhancing the adsorption of the anionic dyes (MO and CR).

Co-Br exhibits fast adsorption at an initial dye concentration of 30 mg/L, reaching equilibrium over methylene blue (19.08 mg/g) and Congo red (13.08 mg/g) at 60 min and methyl orange (10.51 mg/g) at 75 min. Similarly, **Co-Cl** reached the same equilibrium time for methylene blue (19.15 mg/g) and Congo red (12.15 mg/g). However, the equilibrium for methyl orange was reached after 150 min (19.00 mg/g). Despite MO being the smallest of the three dyes (1.3 nm), its slower adsorption rate compared to MB (1.4 nm) and CR (2.6 nm) suggests molecular size alone does not govern the adsorption kinetics.

Adsorption was more favorable for the anionic dyes (MO and CR) than for the cationic dye (MB), in agreement with the literature. In the case of anionic dyes (**Figure 32**), common interactions such as electrostatic interactions between the available sites of the MOFs´ central atom and the negatively charged dyes enhanced adsorption to higher values. Additionally, other interactions, including hydrogen bonds and π-π stacking contribute to high adsorption values.

On the other hand, cationic dyes like MB tend to be adsorbed primarily through weaker interactions, including hydrogen bonds and *π-π* stacking, which significantly impact the overall adsorption capacity. The notable difference in q_m between MO and CR can be attributed to variations in their electrostatic interactions with the MOFs. CR has two SO_3^- groups, whereas MO has only one, leading to differences in electrostatic interaction (30). Additionally, CR contains more aromatic rings, which enhance π-π interactions with the imidazole rings.

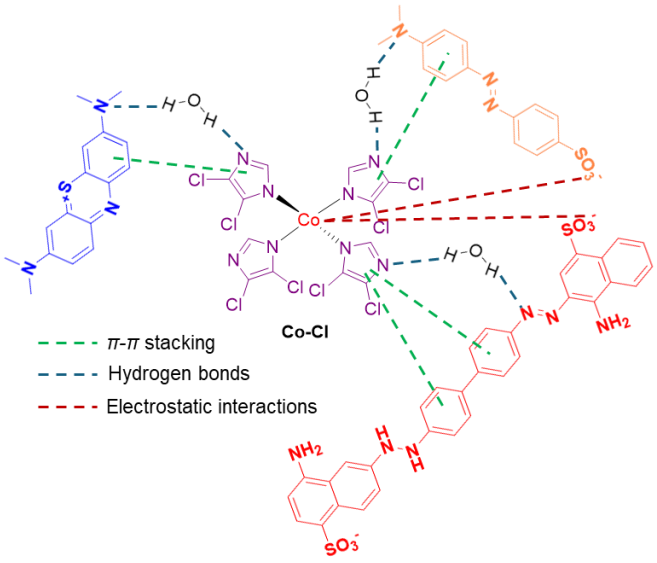

Figure 32. Proposed interaction mechanism for dyes´ adsorption.

CHAPTER 5 CONCLUSIONS

- Ligands **4** and **5** were synthesized and characterized by FTIR, and HRMS. In addition, melting points were determined for its confirmation.
- **Co-Cl** and **Co-Br** were synthesized and characterized by PXRD, nitrogen physisorption, PZC (8.4 and 7.9), water contact angle (60° and 75°), and FTIR.
- The MOFs are isostructural of **ZIF-71** and **ZIF-71(ClBr)** exhibiting similar X-ray patterns and BET surface areas (924 m^2/g and 706 m^2/g).
- MOFs exhibit high adsorption capacities at pH 8 for MB and pH 4 for MO and CR.
- Kinetics analysis showed that MB and CR adsorption is fitted well with the PS-2 model for both **Co-Cl** and **Co-Br**. On the other hand, adsorption of MO followed the PS-1 model.
- Experimentally, the q_m for MB, MO, and CR were 119 mg/g, 265 mg/g, and 1803 mg/g for **Co-Cl**. In the case of **Co-Br**, the results were 61 mg/g, 247 mg/g, and 2100 mg/g. These results surpass the adsorption capacities of **ZIF-8** and **ZIF-67** for MB and CR adsorption. However, under the experimental conditions studied, MO adsorption did not exceed the values observed for **ZIF-8** and **ZIF-67**.
- Adsorption-desorption cycles provided insights into the regeneration capability of these MOFs.
- The study primarily focuses on batch adsorption under controlled conditions, which may not fully replicate real cases involving complex dye industrial effluents. Future work should explore the performance under different temperatures and dynamic adsorption systems.

REFERENCES

1. World Health Organization. Sustainable Development Goals [Internet]. [cited 2025 Aug 5]. Available from: https://www.un.org/sustainabledevelopment/water-and-sanitation/#:~:text=Goal%206%20targets-,Facts%20and%20figures,significant%20risks%20to%20social%20stability.

2. Ewuzie U, Saliu OD, Dulta K, Ogunniyi S, Bajeh AO, Iwuozor KO, et al. A review on treatment technologies for printing and dyeing wastewater (PDW). Journal of Water Process Engineering. 2022;50:103273.

3. Oladoye PO, Ajiboye TO, Omotola EO, Oyewola OJ. Methylene blue dye: Toxicity and potential elimination technology from wastewater. Results in Engineering. 2022;16:100678.

4. Mohamed EA, Ahmed HM, Altalhi AA, Al-Shamiri HAS, Negm NA. Highly efficient and rapid removal of Congo red dye from textile wastewater using facile synthesized Mg/Ni/Al layered double hydroxide. Sci Rep. 2025;15(1):2183.

5. Kishor R, Purchase D, Saratale GD, Romanholo Ferreira LF, Hussain CM, Mulla SI, et al. Degradation mechanism and toxicity reduction of methyl orange dye by a newly isolated bacterium Pseudomonas aeruginosa MZ520730. Journal of Water Process Engineering. 2021;43:102300.

6. Lellis B, Fávaro-Polonio CZ, Pamphile JA, Polonio JC. Effects of textile dyes on health and the environment and bioremediation potential of living organisms. Biotechnology Research and Innovation. 2019;3(2):275–90.

7. Al-Tohamy R, Ali SS, Li F, Okasha KM, Mahmoud YAG, Elsamahy T, et al. A critical review on the treatment of dye-containing wastewater: Ecotoxicological and health concerns of textile dyes and possible remediation approaches for environmental safety. Ecotoxicol Environ Saf. 2022;231:113160.

8. Rafatullah M, Sulaiman O, Hashim R, Ahmad A. Adsorption of methylene blue on low-cost adsorbents: A review. Vol. 177, Journal of Hazardous Materials. 2010. p. 70–80.

9. Kant R. Adsorption of Dye Eosin from an Aqueous Solution on two Different Samples of Activated Carbon by Static Batch Method. J Water Resour Prot. 2012;04(02):93–8.

10. Ramutshatsha-Makhwedzha D, Mavhungu A, Moropeng ML, Mbaya R. Activated carbon derived from waste orange and lemon peels for the adsorption of methyl orange and methylene blue dyes from wastewater. Heliyon. 2022 Aug 1;8(8).

11. Shitu A, Ibrahim A. Removal of methylene blue using low cost adsorbent: a review [Internet]. Vol. 4, Research Journal of Chemical Sciences. 2014. Available from: www.isca.me

12. Arora C, Soni S, Sahu S, Mittal J, Kumar P, Bajpai PK. Iron based metal organic framework for efficient removal of methylene blue dye from industrial waste. J Mol Liq. 2019 Jun 15;284:343–52.

13. Feng Y, Li Y, Xu M, Liu S, Yao J. Fast adsorption of methyl blue on zeolitic imidazolate framework-8 and its adsorption mechanism. RSC Adv. 2016;6(111):109608–12.

14. Huhtamäki T, Tian X, Korhonen JT, Ras RHA. Surface-wetting characterization using contact-angle measurements. Nat Protoc. 2018;13(7):1521–38.

15. Nagy N. Contact Angle Determination on Hydrophilic and Superhydrophilic Surfaces by Using *r* –θ-Type Capillary Bridges. Langmuir. 2019;35(15):5202–12.

16. Yin H, Cay-Durgun P, Lai T, Zhu G, Engebretson K, Setiadji R, et al. Effect of ZIF-71 ligand-exchange surface modification on biofuel recovery through pervaporation. Polymer (Guildf). 2020;195:122379.

17. Tiempos-Flores N, Hernández-Fernández E, Rico-Barragan A, Raziel Álvarez J, Juárez-Ramírez I, Garza-Navarro MA, et al. Enhanced hydrophobicity of modified ZIF-71 metal-organic framework for biofuel purification. Polyhedron. 2022 May 1;217:115736.

18. Chakraborty T, Das M, Lin CY, Su Y, Yuan B, Kao CH. ZIF-8 Nanoparticles Based Electrochemical Sensor for Non-Enzymatic Creatinine Detection. Membranes (Basel). 2022 Jan 28;12(2):159.

19. Banerjee R, Phan A, Wang B, Knobler C, Furukawa H, O'Keeffe M, et al. High-Throughput Synthesis of Zeolitic Imidazolate Frameworks and Application to CO_2 Capture. Science (1979). 2008 Feb 15;319(5865):939–43.

20. Santoso E, Ediati R, Istiqomah Z, Sulistiono DO, Nugraha RE, Kusumawati Y, et al. Facile synthesis of ZIF-8 nanoparticles using polar acetic acid solvent for enhanced adsorption of methylene blue. Microporous and Mesoporous Materials. 2021 Jan 1;310:110620.

21. Nian P, Ma C, Liu H, Qiu J, Zhang X. High-Performance Co-Based ZIF-67 Tubular Membrane Achieved by ZnO-Induced Synthesis for Highly Efficient Pervaporation Separation of Methanol/Methyl *tert* -Butyl Ether Mixture. Ind Eng Chem Res. 2019;58(33):15297–306.

22. Li H, Shi W, Du Q, Huang S, Zhang H, Zhou R, et al. Removal of high concentration Congo red by hydrophobic PVDF hollow fiber composite membrane coated with a loose and porous ZIF-71PVDF layer through vacuum membrane distillation. Journal of Industrial Textiles. 2022;51(5):7641S-7673S.

23. Mohamed F, Shaban M, Zaki SK, Abd-Elsamie MS, Sayed R, Zayed M, et al. Activated carbon derived from sugarcane and modified with natural zeolite for efficient adsorption of methylene blue dye: experimentally and theoretically approaches. Sci Rep. 2022 Dec 1;12(1).

24. El-Bery HM, Saleh M, El-Gendy RA, Saleh MR, Thabet SM. High adsorption capacity of phenol and methylene blue using activated carbon derived from lignocellulosic agriculture wastes. Sci Rep. 2022 Dec 1;12(1).

25. Nazir MA, Khan NA, Cheng C, Shah SSA, Najam T, Arshad M, et al. Surface induced growth of ZIF-67 at Co-layered double hydroxide: Removal of methylene blue and methyl orange from water. Appl Clay Sci. 2020 Jun 1;190:105564.

26. Zhan Y, Guan X, Ren E, Lin S, Lan J. Fabrication of zeolitic imidazolate framework-8 functional polyacrylonitrile nanofibrous mats for dye removal. Journal of Polymer Research. 2019;26(6):145.

27. Bestani B, Benderdouche N, Benstaali B, Belhakem M, Addou A. Methylene blue and iodine adsorption onto an activated desert plant. Bioresour Technol. 2008;99(17):8441–4.

28. Nazir MA, Bashir MA, Najam T, Javed MS, Suleman S, Hussain S, et al. Combining structurally ordered intermetallic nodes: Kinetic and isothermal studies for removal of malachite green and methyl orange with mechanistic aspects. Microchemical Journal. 2021 May 1;164.

29. Martini BK, Daniel TG, Corazza MZ, De Carvalho AE. Methyl orange and tartrazine yellow adsorption on activated carbon prepared from boiler residue: Kinetics, isotherms, thermodynamics studies and material characterization. J Environ Chem Eng. 2018 Oct 1;6(5):6669–79.

30. Zhang Z hang, Zhang J li, Liu J ming, Xiong Z hu, Chen X. Selective and Competitive Adsorption of Azo Dyes on the Metal–Organic Framework ZIF-67. Water Air Soil Pollut. 2016;227(12):471.

31. Ahmad Aftab R, Zaidi S, Aslam Parwaz Khan A, Arish Usman M, Khan AY, Tariq Saeed Chani M, et al. Removal of congo red from water by adsorption onto activated carbon derived from waste black cardamom peels and machine learning modeling. Alexandria Engineering Journal. 2023;71:355–69.

32. Aminu I, Gumel SM, Ahmad WA, Idris AA. Adsorption Isotherms and Kinetic Studies of Congo-Red Removal from Waste Water Using Activated Carbon Prepared from Jujube Seed. Am J Analyt Chem. 2020;11(01):47–59.

33. Thanh Tu NT, Thien TV, Du PD, Thanh Chau VT, Mau TX, Khieu DQ. Adsorptive removal of Congo red from aqueous solution using zeolitic imidazolate framework–67. J Environ Chem Eng. 2018;6(2):2269–80.

34. Jiang C, Fu B, Cai H, Cai T. Efficient adsorptive removal of Congo red from aqueous solution by synthesized zeolitic imidazolate framework-8. Chemical Speciation & Bioavailability. 2016;28(1–4):199–208.

35. Purkait MK, Maiti A, DasGupta S, De S. Removal of congo red using activated carbon and its regeneration. J Hazard Mater. 2007;145(1–2):287–95.

36. World Health Organization. Drinking water [Internet]. 2023 [cited 2025 Jan 3]. Available from: https://www.who.int/news-room/fact-sheets/detail/drinking-water

37. Zare EN, Mudhoo A, Khan MA, Otero M, Bundhoo ZMA, Navarathna C, et al. Water decontamination using bio-based, chemically functionalized, doped, and ionic liquid-enhanced adsorbents: review. Environ Chem Lett. 2021;19(4):3075–114.

38. Mexico Government. LEY GENERAL DEL EQUILIBRIO ECOLOGICO Y LA PROTECCION AL AMBIENTE. 2024.

39. Wang J, Zhu X, Dai Y, Xu M, Wang D, Han Y, et al. Health Risk of Heavy Metals in Drinking Water Sources of Water-Carrying Lakes Affected by Retreating Polder: A Case Study of Luoma Lake. Water (Basel). 2024;16(18):2699.

40. Dutta S, Adhikary S, Bhattacharya S, Roy D, Chatterjee S, Chakraborty A, et al. Contamination of textile dyes in aquatic environment: Adverse impacts on aquatic ecosystem and human health, and its management using bioremediation. J Environ Manage. 2024;353:120103.

41. Sharma A, Kumar V, Shahzad B, Tanveer M, Sidhu GPS, Handa N, et al. Worldwide pesticide usage and its impacts on ecosystem. SN Appl Sci. 2019;1(11):1446.

42. Li Y, Guo R, Liang X, Yao B, Yan S, Guo Y, et al. Pollution characteristics, ecological and health risks of herbicides in a drinking water source and its inflowing rivers in North China. Environmental Pollution. 2023;334:122130.

43. Muambo KE, Kim MG, Kim DH, Park S, Oh JE. Pharmaceuticals in raw and treated water from drinking water treatment plants nationwide: Insights into their sources and exposure risk assessment. Water Res X. 2024;24:100256.

44. Tejada-Tovar C, Villabona-Ortíz Á, Ortega-Toro R. Removal of Metals and Dyes in Water Using Low-Cost Agro-Industrial Waste Materials. Applied Sciences. 2023;13(14):8481.

45. Nikfar S, Jaberidoost M. Dyes and Colorants. In: Encyclopedia of Toxicology. Elsevier; 2014. p. 252–61.

46. Uddin MJ, Ampiaw RE, Lee W. Adsorptive removal of dyes from wastewater using a metal-organic framework: A review. Vol. 284, Chemosphere. Elsevier Ltd; 2021.

47. CRINI G. Non-conventional low-cost adsorbents for dye removal: A review. Bioresour Technol. 2006;97:1061–85.

48. Dutta S, Gupta B, Srivastava SK, Gupta AK. Recent advances on the removal of dyes from wastewater using various adsorbents: a critical review. Mater Adv. 2021;2(14):4497–531.

49. Arora C, Soni S, Sahu S, Mittal J, Kumar P, Bajpai PK. Iron based metal organic framework for efficient removal of methylene blue dye from industrial waste. J Mol Liq. 2019;284:343–52.

50. Butova V v, Soldatov MA, Guda AA, Lomachenko KA, Lamberti C. Metal-organic frameworks: structure, properties, methods of synthesis and characterization. Russian Chemical Reviews. 2016 Mar 31;85(3):280–307.

51. Long JR, Yaghi OM. The pervasive chemistry of metal–organic frameworks. Chem Soc Rev. 2009;38(5):1213.

52. Atlas of Zeolite Framework Types. Elsevier; 2001.

53. Zhou HC, Long JR, Yaghi OM. Introduction to Metal–Organic Frameworks. Chem Rev. 2012;112(2):673–4.

54. Chen Z, Qing H, Zhou K, Sun D, Wu R. Metal-organic framework-derived nanocomposites for electrocatalytic hydrogen evolution reaction. Prog Mater Sci. 2020;108:100618.

55. Kaneti YV, Dutta S, Hossain MSA, Shiddiky MJA, Tung KL, Shieh FK, et al. Strategies for Improving the Functionality of Zeolitic Imidazolate Frameworks: Tailoring Nanoarchitectures for Functional Applications. Advanced Materials. 2017 Oct 11;29(38).

56. Phan A, Doonan CJ, Uribe-Romo FJ, Knobler CB, Okeeffe M, Yaghi OM. Synthesis, structure, and carbon dioxide capture properties of zeolitic imidazolate frameworks. Acc Chem Res. 2010 Jan 19;43(1):58–67.

57. Yurkanis P. Quimica Organica Yurkanis. 5th ed. Santa Barbara;

58. Yadav LDS. Organic Spectroscopy. Dordrecht: Springer Netherlands; 2005.

59. Holder CF, Schaak RE. Tutorial on Powder X-ray Diffraction for Characterizing Nanoscale Materials. ACS Nano. 2019;13(7):7359–65.

60. Cychosz KA, Thommes M. Progress in the Physisorption Characterization of Nanoporous Gas Storage Materials. Engineering. 2018;4(4):559–66.

61. Sing KSW. Physisorption of nitrogen by porous materials. Journal of Porous Materials. 1995;2(1):5–8.

62. Al-Maliky EA, Gzar HA, Al-Azawy MG. Determination of Point of Zero Charge (PZC) of Concrete Particles Adsorbents. IOP Conf Ser Mater Sci Eng. 2021;1184(1):012004.

63. Slesinska S, Galek P, Menzel J, Donne SW, Fic K, Płatek-Mielczarek A. Fundamentals and Implication of Point of Zero Charge (PZC) Determination

for Activated Carbons in Aqueous Electrolytes. Advanced Science. 2024;11(48):2409162.

64. Bakatula EN, Richard D, Neculita CM, Zagury GJ. Determination of point of zero charge of natural organic materials. Environmental Science and Pollution Research. 2018;25(8):7823–33.

65. Cwalinski T, Polom W, Marano L, Roviello G, D'Angelo A, Cwalina N, et al. Methylene Blue—Current Knowledge, Fluorescent Properties, and Its Future Use. J Clin Med. 2020 Nov 2;9(11):3538.

66. Azami M, Bahram M, Nouri S, Naseri A. Central composite design for the optimization of removal of the azo dye, methyl orange, from waste water using fenton reaction. Journal of the Serbian Chemical Society. 2012;77(2):235–46.

67. Jung C, Rhee J Il, Yoo D Il, Shin Y. Application of Fluorescence Spectroscopy in Indigo Reduction Process : Identification of Reduction Stages and Reduced Indigo Concentration. Fibers and Polymers. 2022 Jan 1;23(1):127–35.

68. Groom CR, Bruno IJ, Lightfoot MP, Ward SC. The Cambridge Structural Database. Acta Crystallogr B Struct Sci Cryst Eng Mater. 2016;72(2):171–9.

69. Thommes M, Kaneko K, Neimark A V., Olivier JP, Rodriguez-Reinoso F, Rouquerol J, et al. Physisorption of gases, with special reference to the evaluation of surface area and pore size distribution (IUPAC Technical Report). Pure and Applied Chemistry. 2015;87(9–10):1051–69.

70. Li W, Zhang Q, Zhang J, Zheng Y, Zhang H, Liu J, et al. Fabrication of hydrophobic regenerated activated carbon with high specific surface area. J Mater Sci. 2021 Dec 1;56(36):19969–82.

71. Putra Hidayat AR, Zulfa LL, Widyanto AR, Abdullah R, Kusumawati Y, Ediati R. Selective adsorption of anionic and cationic dyes on mesoporous UiO-66 synthesized using a template-free sonochemistry method: kinetic, isotherm and thermodynamic studies. RSC Adv. 2023;13(18):12320–43.

72. Uddin MdT, Rahman MdA, Rukanuzzaman Md, Islam MdA. A potential low cost adsorbent for the removal of cationic dyes from aqueous solutions. Appl Water Sci. 2017;7(6):2831–42.

73. Andriyko L, Kurbanov M, Siora I, Petrik I, Marynin A, Tulaganov S. The influence of the aqueous media acidity on the electrokinetic potential, aggregation and adsorption properties of silica nanoparticles synthesized from metallurgical wastes. J Mol Liq. 2023;392:123513.

74. Li Y, Gao C, Jiao J, Cui J, Li Z, Song Q. Selective Adsorption of Metal–Organic Framework toward Methylene Blue: Behavior and Mechanism. ACS Omega. 2021;6(49):33961–8.

75. Soni S, Bajpai PK, Mittal J, Arora C. Utilisation of cobalt doped Iron based MOF for enhanced removal and recovery of methylene blue dye from waste water. J Mol Liq. 2020;314:113642.

76. Daneshgar H, Sojdeh S, Salehi G, Edrisi M, Bagherzadeh M, Rabiee N. Comparative study of synthesis methods and pH-dependent adsorption of methylene blue dye on UiO-66 and NH2-UiO-66. Chemosphere. 2024;353:141543.

77. Wang J, Tan Y, Yang H, Zhan L, Sun G, Luo L. On the adsorption characteristics and mechanism of methylene blue by ball mill modified biochar. Sci Rep. 2023;13(1):21174.

78. Qiu J, Feng Y, Zhang X, Jia M, Yao J. Acid-promoted synthesis of UiO-66 for highly selective adsorption of anionic dyes: Adsorption performance and mechanisms. J Colloid Interface Sci. 2017;499:151–8.

79. Zhang X, Qian L, Yang S, Peng Y, Xiong B, Li J, et al. Comparative studies of methyl orange adsorption in various metal-organic frameworks by nitrogen adsorption and positron annihilation lifetime spectroscopy. Microporous and Mesoporous Materials. 2020;296:109993.

80. Luo Y, Chen D, Wei F, Liang Z. Synthesis of Cu-BTC Metal-Organic Framework by Ultrasonic Wave-Assisted Ball Milling with Enhanced Congo Red Removal Property. ChemistrySelect. 2018;3(41):11435–40.

81. Assafi A, El Hadj Ali YA, Almufarij RS, Hejji L, Raza N, Villarejo LP, et al. Ultrasound-assisted adsorption of organic dyes in real water samples using zirconium (IV)-based metal-organic frameworks UiO-66-NH2 as an adsorbent. Heliyon. 2023;9(11):e22001.

82. Dong X, Lin Y, Ma Y, Zhao L. N-contaning UiO-67 derived multifunctional hybrid materials as highly effective adsorbents for removal of Congo red. Inorganica Chim Acta. 2020;510:119748.

83. Moradi SE, Dadfarnia S, Haji Shabani AM, Emami S. Removal of congo red from aqueous solution by its sorption onto the metal organic framework MIL-100(Fe): equilibrium, kinetic and thermodynamic studies. Desalination Water Treat. 2015;56(3):709–21.

84. Sudarsan S, Murugesan G, Varadavenkatesan T, Vinayagam R, Selvaraj R. Efficient adsorptive removal of Congo Red dye using activated carbon derived from Spathodea campanulata flowers. Sci Rep. 2025;15(1):1831.

85. Liu P, Song T, Deng R, Hou X, Yi J. The efficient removal of congo red and ciprofloxacin by peony seeds shell activated carbon with ultra-high specific surface area. Environmental Science and Pollution Research. 2023;30(18):53177–90.